

Pulse-Period – Moment-Magnitude Relations Derived with Wavelet Analysis and their Relevance to Estimate Structural Deformations

Eleftheria Efthymiou¹ and Nicos Makris^{1,2,*}

¹*Dept. of Civil & Environmental Engineering, Southern Methodist University, Dallas, TX, 75276*

²*Office of Theoretical and Applied Mechanics, Academy of Athens, 106 79, Greece*

*nmakris@smu.edu

Abstract

Motivated from the quadratic dependence of peak structural displacements to the pulse period, T_p , of pulse-like ground motions, this paper revisits the pulse-period – moment-magnitude (T_p – M_W) relations of ground motions generated from near-source earthquakes with epicentral distances, $D \leq 20$ km. A total of 1260 ground motions are interrogated with wavelet analysis to identify energetic acceleration pulses (not velocity pulses) and extract their optimal period, T_p , amplitude, a_p , phase, ϕ and number of half-cycles, γ . The interrogation of acceleration records with wavelet analysis is capable of extracting shorter-duration distinguishable pulses with engineering significance, which override the longer near-source pulses and they are not necessarily of random character. Our wavelet analysis identified 109 pulse-like records from normal faults, 188 pulse-like records from reverse faults and 125 pulse-like records from strike-slip faults, all with epicentral distances $D \leq 20$ km. Regression analysis on the extracted data concluded that the same T_p – M_W relation can be used for pulse-like ground motions generated either from strike-slip faults or from dip-slip normal faults; whereas, a different T_p – M_W relation is proposed for dip-slip reverse faults. The study concludes that for the same moment magnitude, M_W , the pulse periods of ground motions generated from strike-slip faults are on average larger than these from reverse faults — a result that is in agreement with findings from past investigations. Most importantly, our wavelet analysis on acceleration records produces T_p – M_W relations with a slope that is lower than the slopes of the T_p – M_W relations presented by past investigators after merely fitting velocity pulses. As a result, our proposed T_p – M_W relations yield lower T_p values for larger-magnitude earthquakes (say $M_W > 6$), allowing for the estimation of dependable peak structural displacements that scale invariably with $a_p T_p^2$.

1 Introduction

One of the important challenges in earthquake engineering is the estimation of peak inelastic structural displacements for collapse prevention and avoidance of irreparable damage. Traditionally, earthquake shaking was viewed as a random motion characterized essentially by two parameters: (a) its peak ground acceleration (PGA); and (b) its overall duration, T_D , and this led to the world-wide accepted equivalent static lateral force procedure (UBC 1997, FEMA-273 1997, IBC 2000, FEMA 2000). Fourier spectra of excitations have been shown occasionally in technical publications; yet, the frequency content of ground motions was a concern only in the design of special projects. The random character of earthquake excitations was bypassed in engineering design by establishing the design elastic response spectrum with a horizontal constant value from low to medium periods and a descending tail at longer periods, so that any candidate seismic motion used for the structural response analysis at a given site has to be compatible to the extent possible with the proposed design spectrum.

The strong motion recorded by the United States Coast and Geodetic Survey (USCGS) accelerometer at Port Hueneme, California on March 18, 1957 was the first recorded strong seismic motion which consisted essentially of a single pulse (Housner and Hudson 1958). Figure 1 plots the North–South component of the ground motion recorded during the 1957 Port Hueneme earthquake (thin solid lines) together with the best fit of a mathematical wavelet (Vassiliou and Makris 2011) on the acceleration record with a pulse period $T_p = 0.65$ s and an acceleration pulse amplitude, $a_p = 0.16g$ (heavy solid lines). In their insightful paper Housner and Hudson (1958) indicate that the elastic response spectrum values from the 1957 Port Hueneme record (also shown in Fig. 1 (bottom)) are considerably larger than the values from the spectra of most typical Pacific Coast earthquakes of equivalent magnitude. These abnormally high-values were reflected in an unusual amount of structural damage from an earthquake of magnitude 4.7 (Housner and Hudson 1958).

The USCGS strong motion accelerometer was approximately 5 miles northwest of the earthquake epicenter, and the 1957 Port Hueneme record marks the beginning of a series of investigations on the pulse-like nature of near-source ground motions (Bolt 1971, 1975) and the severe inelastic displacement demand on structures that result from the coherent, long-duration acceleration pulses (Bertero *et al.* 1976, 1978, 1991, Somerville and Graves 1993). Such investigations

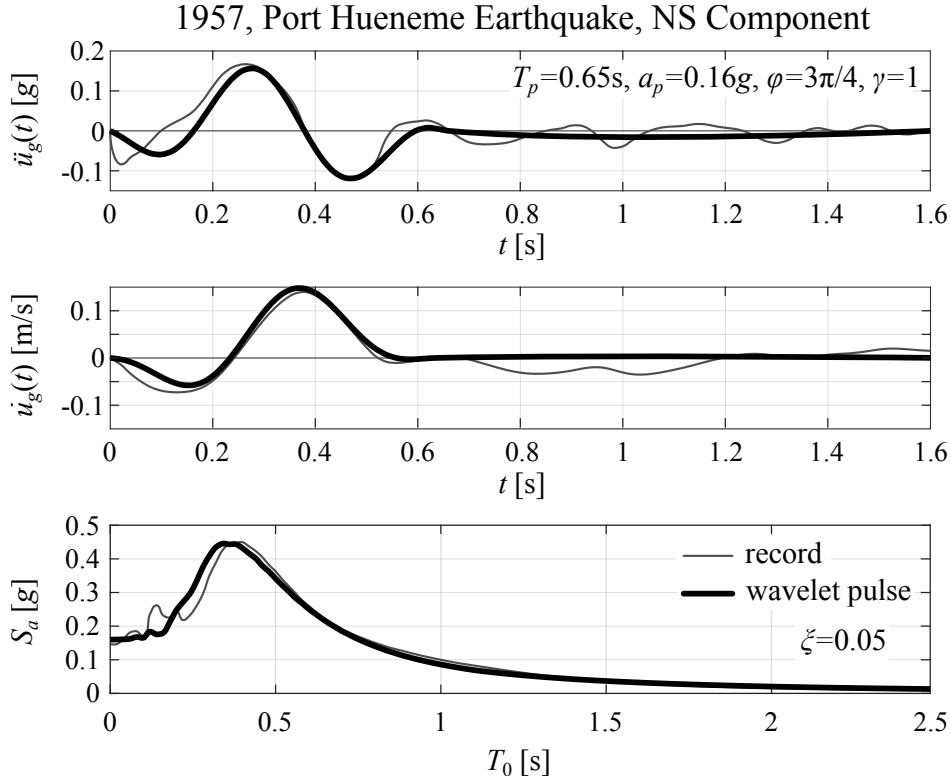


Figure 1: Acceleration and velocity time histories together with the associated elastic acceleration response spectra of the North–South record from the March 18, 1957 Port Hueneme, California earthquake (thin solid lines) and of a wavelet pulse that best fits the acceleration record (heavy solid lines (Vassiliou and Makris 2011)).

were drastically intensified after the 1994 Northridge, California, the 1995 Kobe, Japan, the 1999 Izmit, Turkey and the 1999 Chi-Chi, Taiwan earthquakes which resulted in a large collection of pulse-like ground motions recorded near the causative faults (Hall *et al.* 1995, Makris 1997, Loh *et al.* 2000, Makris and Chang 2000, Ma *et al.* 2001, Wang *et al.* 2001, Sekiguchi and Iwata 2002, and references reported therein).

Less than a decade after the Housner and Hudson (1958) seminal paper, the $M_W = 6.2$, 1966 Parkfield, California earthquake generated ground shaking that was recorded by an array of five strong-motion accelerographs across the San Andreas fault at Cholame. Among the records, the most notable one is the C02 record at a distance of only 80 m from the fault rupture. Figure 2 plots the N65E component of the C02 record together with the best fit of a mathematical wavelet (Vassiliou and Makris 2011) on the acceleration record. The response spectra for this motion were first presented by Housner and Trifunac (1967) (also shown at the bottom of Fig. 2) who indicated

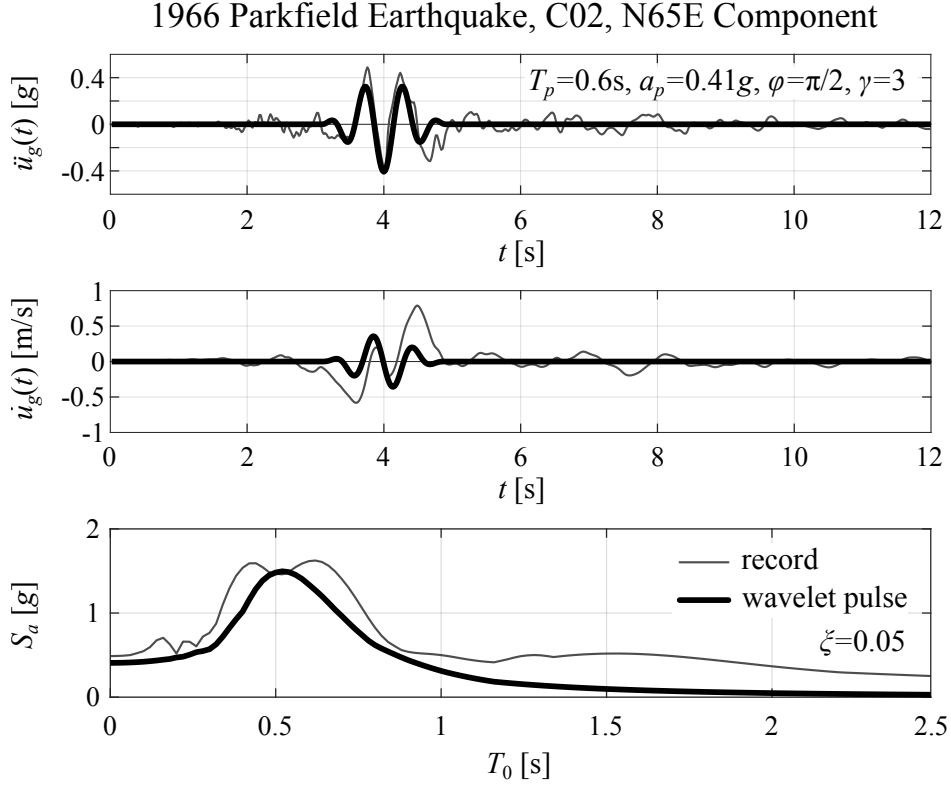


Figure 2: Acceleration and velocity time histories together with the associated elastic acceleration response spectra of the N65E component of the C02 record from the June 28, 1966 Parkfield, California earthquake (thin solid lines) and of a wavelet pulse that best fits the acceleration record (heavy solid lines (Vassiliou and Makris 2011)).

that in an engineering sense the 1966 Parkfield ground motion belongs to a different class than the other strong ground motions recorded before that time; given the $T_p = 0.6$ -s long coherent acceleration pulse that dominates the acceleration record.

The first systematic work on the response of an elastoplastic single-degree-of-freedom (SDoF) structure subjected to pulse-type ground shaking was presented in the papers by Veletsos and Newmark (1960) and Veletsos *et al.* (1965). An early solution to the response of a rigid-plastic system (rigid mass sliding on its moving base with coefficient of friction, μ) subjected to a rectangular acceleration pulse with amplitude a_p and duration T_p was presented in Newmark's (1965) Rankine Lecture who showed that the maximum sliding displacement of a mass relative to its shaking base is

$$u_{\max} = \frac{a_p T_p^2}{2} \left(\frac{a_p}{\mu g} - 1 \right), \quad a_p > \mu g \quad (1)$$

Equation (1) indicates that the maximum sliding (inelastic) displacement is proportional to the

pulse acceleration a_p (that is the PGA for a rectangular pulse); and most importantly, is proportional to the square of the duration of the pulse (pulse period) T_p^2 . The product $a_p T_p^2 = L_p$ in front of the parenthesis of Eq. (1) is a characteristic length scale that expresses the persistence of the pulse to induce inelastic deformations; whereas, the quantity in the parenthesis $\frac{a_p}{\mu g}$ expresses the strength of the pulse. While the rectangular pulse used by [Newmark \(1965\)](#) is not physically realizable by earthquake shaking (results to an infinite ground displacement) it shows in a lucid manner that inelastic deformations are proportional to the square of the duration of the pulse T_p^2 — a physical reality that has been overlooked invariably by seismic codes worldwide for several decades. The scaling of the maximum sliding displacement with T_p^2 shown by Eq. (1) was obtained by [Newmark \(1965\)](#) after integrating the differential equation of motion of the simple rigid-plastic system. The same result can be obtained with dimensional analysis for the response of any given structural system subjected to any pulse-like excitation ([Makris and Black 2004a, b](#)) such as the pulse motions shown in Figs. 1 and 2. Figure 3 plots the normalized maximum inelastic displacement $\Pi_m = \frac{u_{\max}}{a_p T_p^2}$ of an elastoplastic structure subjected to a rectangular pulse (left) and the symmetric acceleration wavelet ($\phi = \pi/2$, $\gamma = 3$) that happens to best match the C02/NE65 acceleration record shown in Fig. 2 (right) as a function of the dimensionless strength $\Pi_Q = \frac{Q}{ma_p}$ for various values of the dimensionless yield displacement $\Pi_y = \frac{u_y}{a_p T_p^2}$. The self-similar solutions approach the rigid-plastic limit as the normalized yield displacement $\Pi_y = \frac{u_y}{a_p T_p^2}$ tends to zero ([Makris and Black 2004a](#)). Figure 3 uncovers that the non-reversing rectangular pulse induces much larger displacements than the wavelet that happens to best match the C02 record shown in Fig. 2 as the strength of the structure reduces.

The scaling of the peak displacement u_{\max} , with T_p^2 derived by [Newmark \(1965\)](#) for a sliding mass is independent of the structural behavior as illustrated in Fig. 3. For instance, in the interest of completeness, consider an elastic SDoF oscillator with mass m , stiffness $k = m\omega_0^2 = m \frac{4\pi^2}{T_0^2}$ and damping constant $c = 2\xi m\omega_0$ that is subjected to a given acceleration pulse with duration T_p and acceleration amplitude a_p . The maximum relative-to-the-ground displacement of the elastic SDoF oscillator, u_{\max} , is a function of four variables:

$$u_{\max} = f(T_0, \xi, a_p, T_p) \quad (2)$$

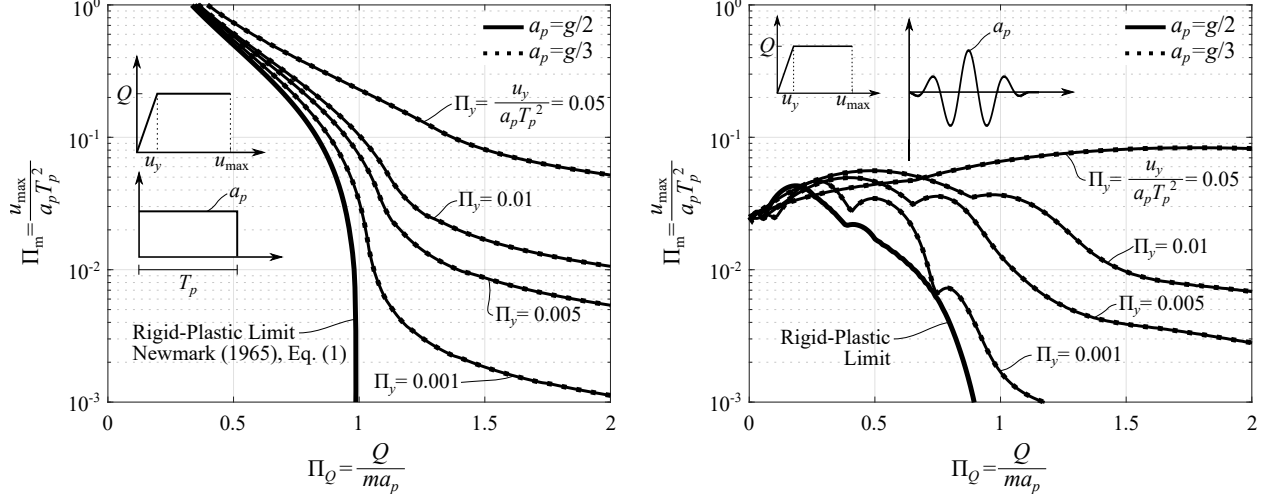


Figure 3: Normalized maximum relative displacement curves $\frac{u_{\max}}{a_p T_p^2}$ of an elastic–plastic structure subjected to a rectangular pulse (left) and a M&P wavelet pulse with $\phi = \pi/2$ and $\gamma = 3$ (right). The self-similar solutions approach the rigid–plastic limit as the normalized yield displacement $\Pi_y = \frac{u_y}{a_p T_p^2}$ tends to zero.

where $T_0 = \frac{2\pi}{\omega_0} = 2\pi\sqrt{\frac{m}{k}}$ and $\xi = \frac{c}{2m\omega_0}$ are the parameters of the elastic structure and a_p and T_p are the parameters of the pulse excitation. The five variables appearing in Eq. (2), $u_{\max} \doteq [L]$, $T_0 \doteq [T]$, $\xi \doteq [1]$, $a_p \doteq [L][T]^{-2}$ and $T_p \doteq [T]$, involve only two reference dimensions, that is length [L] and time [T]. According to the Vaschy – Buckingham Π theorem (Langhaar 1951, Housner and Hudson 1959, Barenblatt 1996), the number of independent dimensionless products (Π -terms) is equal to the number of physical variables appearing in Eq. (2) (5 physical variables) minus the number of reference dimensions (2 reference dimensions [L] and [T]) of the physical problem. Accordingly, for the linear SDoF we have $5-2 = 3$ dimensionless Π -terms and Eq. (2) condenses to:

$$\Pi_m = \frac{u_{\max}}{a_p T_p^2} = \phi\left(\frac{T_0}{T_p}, \xi\right) \quad \text{or} \quad u_{\max} = a_p T_p^2 \phi\left(\frac{T_0}{T_p}, \xi\right) \quad (3)$$

Equations (1) and (3) together with Fig. 3 conclude to the same central result: that regardless whether the structural behavior is rigid-plastic (sliding mass), elastoplastic or elastic, the peak response displacement of any structural system when subjected to a coherent acceleration pulse with duration T_p is proportional to T_p^2 . This result derives directly from dimensional analysis (Makris and Black 2004a) and has been confirmed numerically for reinforced concrete structures (Makris and Psychogios 2006) and steel structures (Karavasilis *et al.* 2010). Consequently, given that the

elastic or inelastic peak structural displacement scales invariably with T_p^2 , the aim of this paper is to produce with wavelet analysis, mathematically-objective T_p - M_W relations after examining their possible dependence on the fault mechanism in an effort to obtain dependable estimates of pulse periods, T_p so that Eq. (3) or the results of Fig. 3 can be used with confidence to estimate structural deformations.

2 Review of Existing $T_p - M_W$ Relations and Problem Statement

A number of models relating the period of the coherent velocity pulse, T_p , to the moment magnitude of the earthquake, M_W are available in the literature. [Somerville \(1998\)](#) examined the period and amplitude of the largest cycle of motion of the fault-normal, forward directivity velocity pulse. This pulse consists of a peak, a trough and three zero crossings. With this idealization, the pulse amplitude is equal to the peak ground velocity (*PGV*) and the pulse period is equal to the duration of the velocity cycle. The proposed model relates the pulse period, T_p , with the earthquake's moment magnitude, M_W , assuming that the period is independent of the distance:

$$\log_{10} T_p = -2.5 + 0.425M_W \quad (4)$$

By constraining the model to be self-similar, [Somerville \(1998\)](#) obtained:

$$\log_{10} T_p = -3.0 + 0.50M_W. \quad (5)$$

[Somerville \(1998\)](#) used records that presented forward directivity only, which are known to produce strong pulses in the fault-normal direction. 15 time histories recorded in close proximity to the earthquakes epicenters: 0–10 km with magnitudes, M_W , between 6.2 and 7.3 were used. The database was complimented by 12 simulated time histories in distance of 3 to 10 km and magnitudes of 6.5 to 7.5. All time-histories are for soil site conditions. A linear relationship between the pulse period T_p and the rise time of slip on the fault, T_R , was identified which is a measure of the duration of slip at a specific point of the fault: $T_p = 2.2T_R$. For a given M_W the rise time in a reverse-faulting earthquake is on average about half that of strike-slip earthquakes, suggesting that the larger ground motion levels of reverse-faulting earthquakes can be attributed to the shorter rise times than strike-slip earthquakes; therefore, the pulse periods, T_p , of pulse-like ground motions from reverse faults are expected to be of shorter duration than the pulse periods of ground motions

from strike-slip faults.

[Krawinkler and Alavi \(1998\)](#) explored the elastic and inelastic dynamic responses of SDoF and MDoF systems subjected to different types of pulse loading. They proposed three different acceleration pulses defined in terms of their period, T_p , and their peak ground acceleration, $a_{g,max}$. The non-differentiable square pulses denoted P1, P2 and P3 correspond to a half-pulse, a full pulse and a multiple pulse, respectively. Pulse P1 is half the P2 pulse. [Alavi and Krawinkler \(2000\)](#) later used the proposed full pulse model P2 to obtain the pulse characteristics of a small set of recorded near-fault ground motions. With regression analysis of the pulse periods of the velocity pulses against the earthquake moment magnitude they obtained:

$$\log_{10} T_p = -1.76 + 0.31M_W \quad (6)$$

where T_p is the pulse period, defined as the duration of the complete velocity cycle and M_W is the moment magnitude of the earthquake. [Alavi and Krawinkler \(2000\)](#) note that the records used in the regression analysis came from different faulting mechanisms and various geology conditions. They also warned that the lack of adequate numbers of recorded near-fault motions suggests that such relationships must be used with caution. However, by cautiously using the proposed relationships and combined with pulse strength demand spectra, one can evaluate the base shear strength required to limit story ductility ratios to specific target values.

In a subsequent paper, [Somerville \(2003\)](#) used a triangular pulse that resembles the P2 velocity pulse of [Krawinkler and Alavi \(1998\)](#) and proposed two additional relationships that relate the period of the largest cycle of the fault-normal velocity waveform that presents forward directivity, T_p , with M_W . The expressions proposed for rock and soil sites assume that the period is independent of the distance from the fault:

$$\log_{10} T_p = \begin{cases} -3.17 + 0.5M_W, & \text{for rock sites} \\ -2.02 + 0.346M_W, & \text{for soil sites} \end{cases} \quad (7)$$

For the rock sites [Somerville \(2003\)](#) proposed a self-similar expression, but for soil sites the expression is allowed to depart from self-similarity to accommodate effects from nonlinear soil response. The soil layers tend to increase the peak velocity and the period of the input rock motion by factors

that depend on the magnitude of the ground motion and on the thickness and the properties of the soil layers (Rodriguez-Marek 2000, Somerville 2003). The two expressions intersect at $M_W = 7.4$ and $T_p = 3.4$ s. Above this point, the relationship for rock sites results in larger T_p than the one for soil sites, although the author states that it is expected that the expression for soil sites would be curved and merge with the expression for rock sites above the intersection point.

Bray and Rodriguez-Marek (2004) examined approximately 50 records presenting forward directivity and proposed a linear relation between $\ln T_p$ and the moment magnitude, M_W after adopting sine pulses to represent simplified velocity-time histories. They distinguished between the fault normal and fault parallel directions of propagation by introducing the time-lag between the initiation of the fault normal and the fault parallel components. They accepted the number of significant pulses as the number of half-cycle velocity pulses that have amplitudes of at least 50% of the PGV of the ground motion. By complementing the work of Somerville (1998), the Bray and Rodriguez-Marek work accounts for distances smaller than 3 km from the fault, which were shown to be of significance, and proposes equations for rock sites, soil sites and for the complete database:

$$\ln T_p = \begin{cases} -6.37 + 1.03M_W, & \text{for all sites} \\ -8.60 + 1.32M_W, & \text{for rock sites} \\ -5.60 + 0.93M_W, & \text{for soil sites} \end{cases} \quad (8)$$

where T_p is the period of the dominant velocity pulse. The regression is constrained to render same periods for rock and soil sites at $M_W = 7.6$ ($T_p = 4.34$ s) in order to avoid obtaining larger periods for rock than for soil when $M_W > 7$.

Mavroeidis and Papageorgiou (2003) indicated that simplified velocity pulses of square or triangular shapes do not adequately capture the time-histories or the response spectra of actual ground motions and their use to study the dynamic responses of structures may result in misleading conclusions. Their work builds on Gabor's (1946) elementary signal, which is essentially a harmonic oscillation within a Gaussian envelope:

$$v(t) = \exp \left[- \left(\frac{2\pi f_p}{\gamma} \right)^2 t^2 \right] \cos(2\pi f_p t + \nu) \quad (9)$$

where f_p is the prevailing frequency of the wavelet, ν is the phase angle and γ controls its oscillatory character. [Mavroeidis and Papageorgiou \(2003\)](#) showed that the Gabor wavelet of Eq. (9) does not allow closed-form solutions for the response of SDoF systems due to the exponential term in the right-hand side of Eq. (9). In the interest of deriving closed-form expressions, they modified Eq. (9) by combining the harmonic oscillation part of the Gabor wavelet ([Gabor 1946](#)), $\cos(2\pi f_p t + \nu)$, with an elevated cosine function of the form:

$$v(t) = \begin{cases} A \frac{1}{2} \left[1 + \cos \left(\frac{2\pi f_p}{\gamma} (t - t_0) \right) \right] \cos[2\pi f_p (t - t_0) + \nu], \\ 0, \text{ otherwise} \end{cases} \quad (10)$$

$$t_0 - \frac{\gamma}{2f_p} \leq t \leq t_0 + \frac{\gamma}{2f_p} \quad \text{with } \gamma > 1 \text{ and } f_p = \frac{1}{T_p}$$

where A and $f_p = 1/T_p$ denote the amplitude and the frequency of the velocity pulse, respectively, ν is the phase of the pulse, γ defines the oscillatory character of the pulse and t_0 defines the time instance when the wavelet is located. The proposed velocity expression of Eq. (10) can capture effectively the displacement, velocity and, in many cases, the acceleration time-histories of recorded earthquakes, and resulted in the following pulse-period–moment–magnitude relation:

$$\log_{10} T_p = -2.2 + 0.4M_W \quad (11)$$

By further accepting self-similar scaling laws between the pulse characteristics and the dimensions of the fault [Mavroeidis and Papageorgiou \(2003\)](#) proposed:

$$\log_{10} T_p = -2.9 + 0.5M_W \quad (12)$$

and they observed that for the same M_W the pulse period is larger on average for strike-slip faults than for reverse faults.

[Fu and Menun \(2004\)](#) after using a similar; yet less sophisticated mathematical expression than Eq. (10) for the velocity pulse, matched synthetic velocity time-histories generated by the Haskell source model ([Aki and Richards 1980](#)), and proposed the following velocity pulse period T_p – moment magnitude M_W relation:

$$\log_{10} T_p = -3.38 + 0.54M_W \quad (13)$$

While the aforementioned studies proposed mathematical expressions of velocity pulses of which the parameters are estimated based on engineering judgement rather than by some formal mathematically objective procedure; the first systematic study for identifying quantitatively coherent velocity pulses in near-fault ground motions was presented by Baker (2007). Baker's work also focuses on velocity pulses and uses wavelet analysis to automatically extract the largest ve-

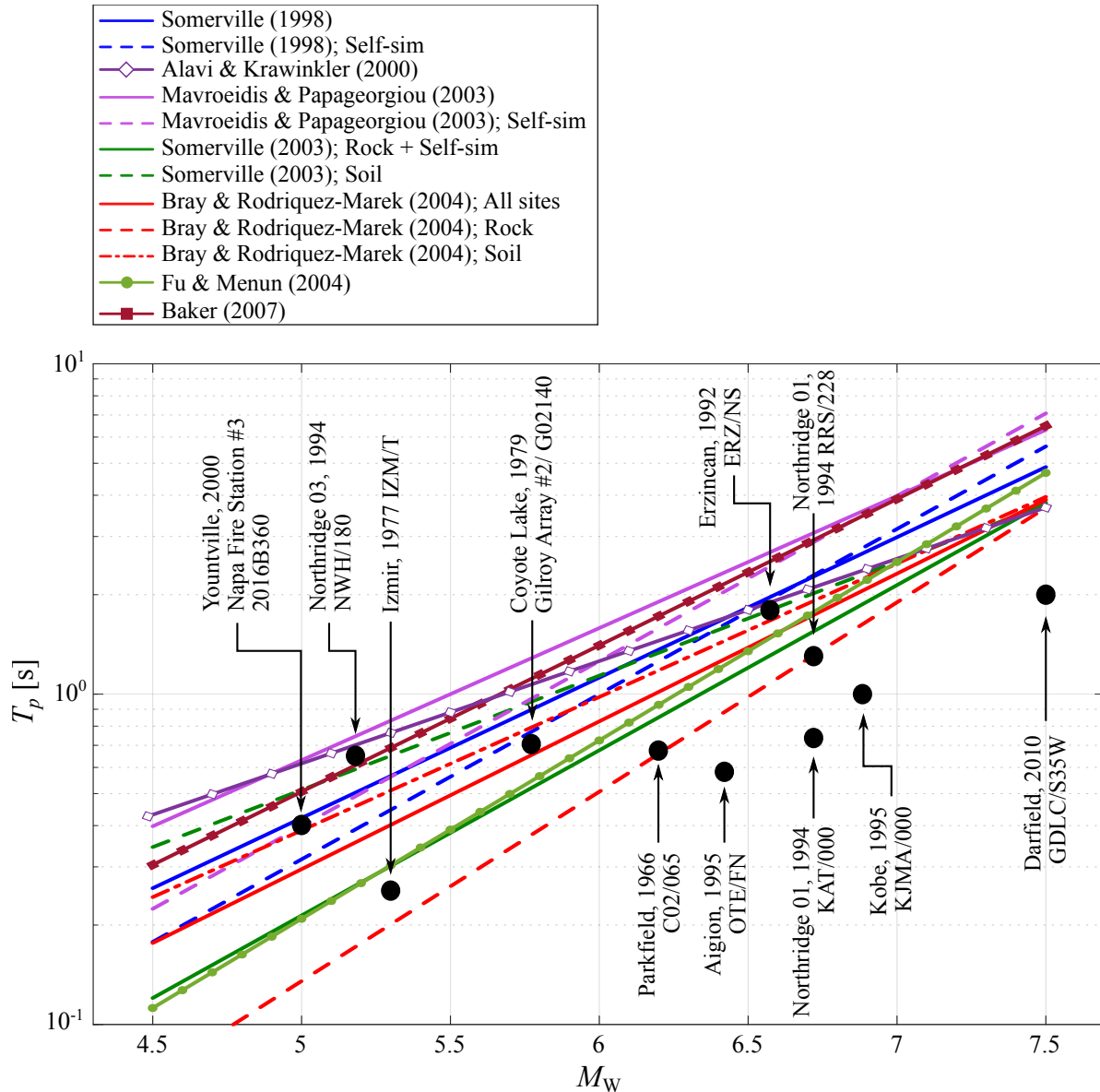


Figure 4: Summary of T_p - M_W relationships known to the literature (Eqs. (4) – (14)) that have been proposed by matching invariably velocity pulses together with the pulse periods of selected historic pulse-like records extracted with wavelet analysis on the acceleration records (Vassiliou and Makris 2011).

locity pulse in a given earthquake record. Baker (2007) employed 4th-order Daubechies wavelets to distil characteristic time- and length-scales from the recorded ground motions. The main limitation of processing velocity (rather than acceleration) time-histories with wavelet analysis is that one can only extract the visible main velocity pulse — that is usually the one associated with the near-source effects. Baker (2007) examined the fault-normal components of 398 earthquakes in the Next Generation Attenuation (NGA) database with $M_W \geq 5.5$ and recorded within 30 km from the fault. He identified 91 pulse-like records; and through regression analysis of the periods of the identified pulses against the corresponding earthquake moment magnitude, proposed the following pulse-period – moment-magnitude relation:

$$E[\ln T_p] = -5.78 + 1.02M_W \quad (14)$$

where $E[\cdot]$ denotes the expected value of $\ln T_p$. The standard deviation of $\ln T_p$ computed by Baker (2007) is $\sigma_{\ln T_p} = 0.55$.

Figure 4 plots the 12 pulse-period – moment-magnitude relations summarized in this section that are all derived invariably by matching velocity pulses of pulse-like ground motions. Clearly, the relations derived for motions recorded on rock offer pulse periods appreciably lower than the other relations; yet, it is worth recognizing that the differences in the values of the pulse periods offered by the relations plotted in Fig. 4 are large. For instance, for an earthquake of magnitude $M_W = 6.0$ the predominant pulse periods range from $T_p \approx 0.5$ s to $T_p \approx 1.6$ s. Given that structural deformations (either elastic or inelastic) scale with T_p^2 (as shown by Eqs. (1), (3) and Fig. 3); when the structural deformations are estimated with $T_p = 0.5$ s, then $u_{\max} \sim 0.5^2 = 0.25$; whereas, when structural deformations are estimated with $T_p = 1.6$ s, then $u_{\max} \sim 1.6^2 = 2.56$ — that is more than a 10-fold increase. This one-order of magnitude variability in the estimation of structural displacements that scale with $a_p T_p^2$ is the main motivation of this work.

Figure 5 plots the acceleration and velocity time histories together with the elastic acceleration spectra of the KAT/000 ground motion recorded during the 1994 Northridge, California $M_W = 6.7$ earthquake (thin solid lines), and of the M&P wavelet with $T_p = 0.74$ s, $a_p = 0.38g$, $\phi = \pi/2$ and $\gamma = 3$ (heavy solid lines) which is a sister wavelet of the best matching wavelet of the C02 record shown in Fig. 2.

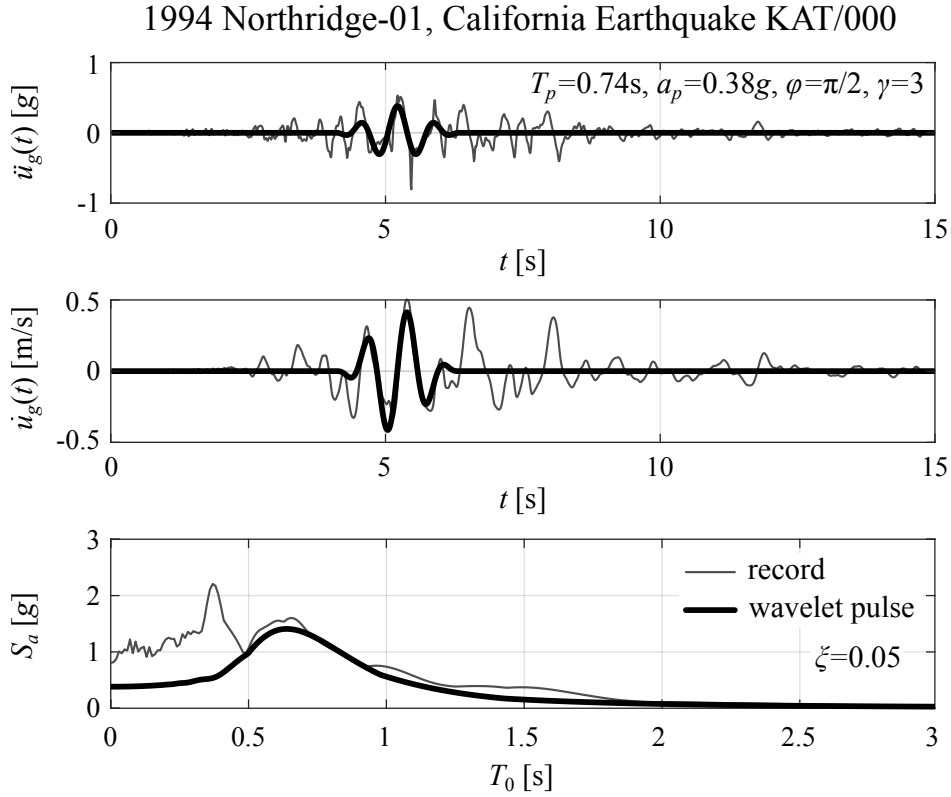


Figure 5: Acceleration and velocity time histories together with the associated elastic acceleration spectra of the KAT/000 record from the 1994 Northridge, California earthquake (thin solid lines) and of the M&P wavelet pulse that best fits the acceleration record (heavy solid lines (Vassiliou and Makris 2011)).

3 On the Engineering Significance of Fitting Velocity Pulses

Figures 1, 2 and 5 show examples of ground motions where the velocity pulse is also distinguishable in the acceleration history, and such ground motions are particularly destructive to the built environment. In other cases, acceleration records contain high-frequency spikes and resemble random motions; however, their velocity and displacements histories uncover a coherent long-duration pulse that results from the non-zero mean of the acceleration fluctuations. As an example, Fig. 6 shows the fault parallel components of the acceleration, velocity and displacement histories of the June 18, 1992 Landers, California earthquake ($M_W = 7.2$) recorded at the Lucerne Valley station (Iwan and Chen 1994). The coherent 7-s long pulse, responsible for the 1.8-m forward displacement, can also be distinguished in the velocity history; whereas the acceleration history is crowded with high-frequency spikes without exhibiting any visible acceleration pulse. The large spectral accelerations in the period range of $T_0 \approx 0.25$ s are due to the high-frequency acceleration spikes;

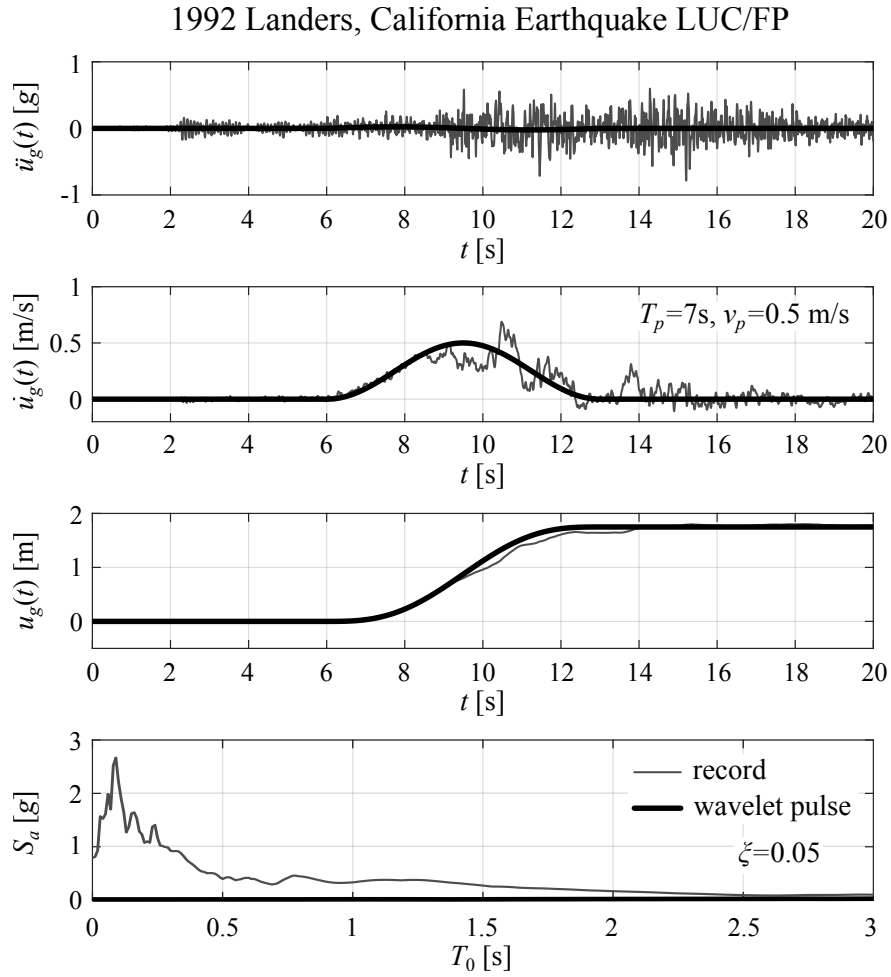


Figure 6: Fault parallel component of the acceleration, velocity and displacement histories together with the elastic acceleration response spectra of the June 18, 1992 Landers, California earthquake ($M_W = 7.2$) recorded at the Lucerne Valley station (thin solid lines) and a one-sine acceleration pulse that captures the long velocity pulse (heavy solid lines).

whereas the 7-s long velocity pulse that creates the “biblical” 1.8-m forward displacement is immaterial to any structure built away from the rupture. A similar situation is shown in Fig. 7 which plots the East–West components of the acceleration, velocity and displacement histories of the August 17, 1999 Kocaeli, Turkey earthquake ($M_W = 7.4$) recorded at the Sakarya station. A coherent 6-s long pulse, responsible for the 2.0-m forward displacement, dominates the velocity time history; however, the acceleration history is crowded with high-frequency spikes without revealing any visible pulse. The large spectra accelerations shown at the bottom of Fig. 7 in the range of $T_0 = 0.25$ s are due to the high-frequency acceleration spikes.

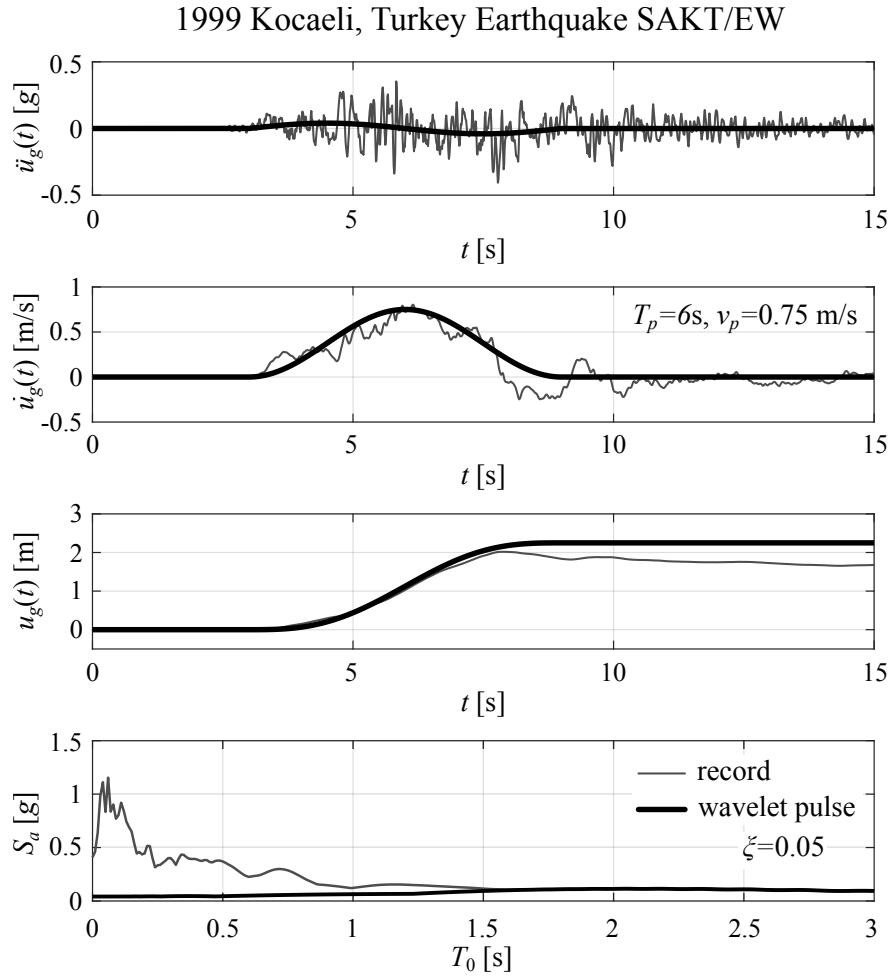


Figure 7: East–West component of the acceleration, velocity and displacement histories together with the elastic acceleration response spectra of the August 17, 1999 Kocaeli, Turkey earthquake ($M_W = 7.4$) recorded at the Sakarya station and a one-sine acceleration pulse that captures the long velocity pulse (heavy solid lines).

Baker (2007) recognized that in several occasions of his velocity-centric analysis (in which all daughter wavelets had the same energy — the default setting in MATLAB (2017) toolbox) the pulse periods obtained from the wavelet analysis differ significantly from the pulse periods obtained from spectral analysis (see Fig. 12 of his paper), and he correctly explained that the pulse period extracted from the peak spectral values is associated in general with the high-frequency oscillatory component of the ground motion; whereas the pulse extracted with the wavelet analysis is associated with the long velocity pulse.

Another situation that challenges the engineering significance of classifying records by only interrogating velocity pulses is that in several near-source records, in addition to the coherent

1999 Chi-Chi, Taiwan Earthquake TCU052/N

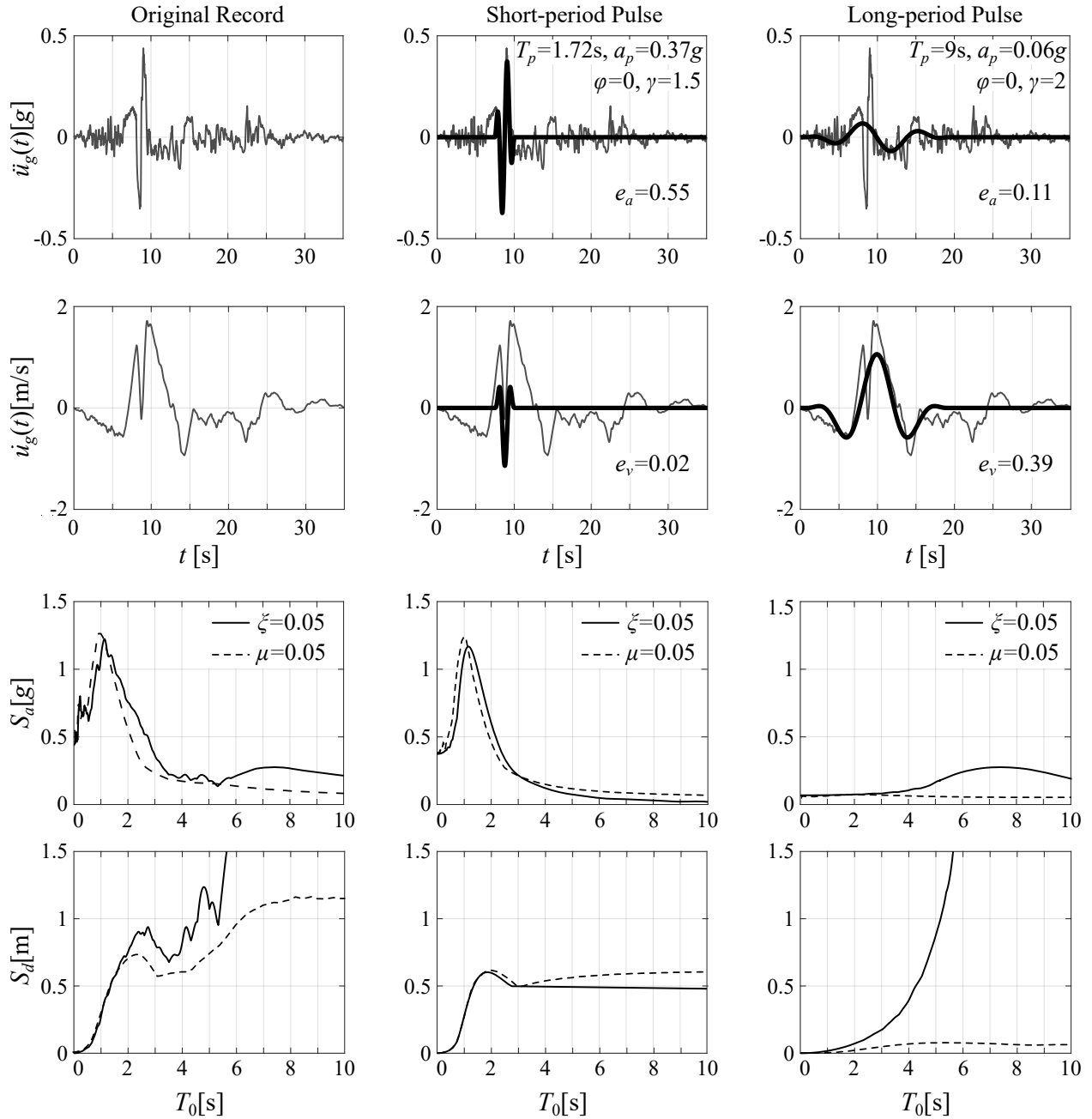


Figure 8: Top: Acceleration, velocity and displacement time histories of the TCU052 North–South component from the 1999 Chi-Chi, Taiwan earthquake. Heavy lines denote the short- and long-duration pulses obtained with wavelet analysis. Bottom: Acceleration and displacement spectra of a linear ($m; k; c$) and a frictional ($m; k; \mu$) oscillator subjected to the recorded motion (left), the short-period pulse (center), and the long-period pulse that is associated with the near-source effects (right).

long-period pulse associated with the near-source effect, there is a shorter duration distinguishable pulse (not necessarily of random character) that overrides the larger duration pulse. These shorter duration overriding pulses may be of significant engineering interest to a wide family of structures and there is a clear need to identify and characterize them. For instance, Fig. 8 shows the North–South component of the acceleration, velocity and displacement histories recorded at TCU052 station during the September 21, 1999 Chi-Chi, Taiwan earthquake. This record contains a 9-s long velocity pulse (the one associated with the near-source effects), which is disturbed by a shorter, distinguishable pulse of duration about 1.7 s. This shorter, overriding pulse is of major engineering significance because it is responsible for most of the base-shear and peak deformations of the majority of structures that are of interest in civil engineering as shown in the elastic and inelastic response spectra shown at the bottom of Fig. 8. Consequently, in order to estimate meaningful structural deformations and base shears it becomes evident that there is a need to extract in a mathematically objective way significant acceleration pulses (not velocity pulses) and construct revised pulse-period – moment-magnitude relations that emerge by best matching acceleration pulses.

4 Extraction of Acceleration Pulses with Wavelet Analysis

In addition to the pressing need to have estimates of pulse period, T_p associated with acceleration pulses, our paper is partly motivated from the observations of [Somerville \(1998\)](#) and [Mavroeidis and Papageorgiou \(2003\)](#) who reported that for the same moment magnitude M_W the pulse periods of ground motions generated from strike-slip faults are on average larger than these from dip-slip

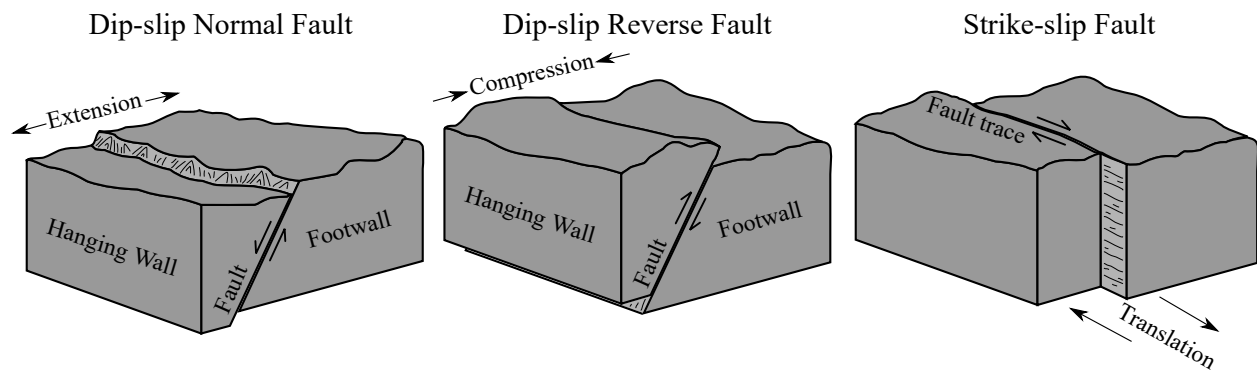


Figure 9: Schematic representation of normal reverse, and strike-slip faults. Normal faults are the result of extension while reverse faults are due to compression. Strike-slip faults are the result of translation between the two fault planes.

reverse faults. Accordingly, a total of 1260 strong-motions with distances from the fault less than 20 km were categorized based on the three faulting mechanisms shown in Fig. 9 — that is a dip-slip normal fault with a downward moving hanging wall, a dip-slip reverse fault with an upward moving hanging wall and strike-slip fault. Among the 1260 strong-motion records, 447 records are generated by normal faults, 478 records are from reverse faults and 335 records are generated from strike-slip faults. From the 1260 records, 748 records are available in the Next Generation Attenuation database (Ancheta *et al.* 2013) and the remaining 512 records are available in the European Strong Motion Database (Ambraseys *et al.* 2002) (see Data and Resources Section).

Forward directivity is observed when the fault rupture propagates towards the site with rupture velocity approximately equal to the shear wave velocity and hence, a coherent and long-period pulse is observed at the beginning of the recorded motion which contains most of the elastic energy. Permanent translation, on the other hand, comes from permanent fault translation as a result of earthquake movement. Previous research studies, such as Somerville (1998, 2003), Mavroeidis and Papageorgiou (2003), Bray and Rodriguez-Marek (2004), focus only on records that presented forward directivity. On the other hand, Baker (2007) did not focus on specific fault mechanisms; yet, acknowledged that a number of the pulse-like earthquake that he identified by wavelet analysis of his database were the result of forward directivity. Following Baker (2007), forward directivity effects have not been used as a criterion to choose the near-fault ground motions included in our database.

The extracted acceleration pulses with wavelet analysis and the resulting velocity pulses have the same effects on the structural response regardless of directivity effects being considered. Wavelets are simple wavelike functions localized on the time axis. For instance, the second derivative of the Gaussian distribution, $e^{-t^2/2}$, known in the seismological literature as the symmetric Ricker wavelet (Ricker 1943, 1944) and widely referred to as the Mexican Hat wavelet (Addison 2002, 2017)

$$\psi(t) = (1 - t^2)e^{-t^2/2} \quad (15)$$

is a wavelike function that can be classified as a wavelet. In order for a wavelike function to be

classified as a wavelet, the wavelike function must have (1) finite energy

$$E = \int_{-\infty}^{\infty} |\psi(t)|^2 dt < \infty \quad (16)$$

and (2) a zero mean.

Our effort concentrates on achieving the best local matching of any given acceleration record with a wavelet that will offer the best estimates of the period ($T_p =$ time scale) and amplitude (a_p , because $a_p T_p^2 =$ length scale) of the prevailing energetic pulse. Accordingly, we perform a series of inner products (convolutions) of the ground acceleration signal, $\ddot{u}_g(t)$, with the wavelet $\psi(t)$ by manipulating the wavelet through a process of translation (i.e., movement along the time axis) and a process of dilation–contraction (i.e. spreading out or squeezing of the wavelet):

$$C(s, \xi) = w(s) \int_0^{\infty} \ddot{u}_g(t) \psi\left(\frac{t - \xi}{s}\right) dt \quad (17)$$

The values of $s = S$ and $\xi = \Xi$ for which the coefficient, $C(s, \xi) = C(S, \Xi)$, reaches the maximum value offer the scale and location of the wavelet $w(s)\psi\left(\frac{t - \xi}{s}\right)$ that locally best matches the acceleration record, $\ddot{u}_g(t)$. Equation (17) is the definition of the wavelet transform (Addison 2017). The quantity $w(s)$ outside the integral in Eq. (17) is a weighting function. Typically, $w(s)$ is set equal to $\frac{1}{\sqrt{s}}$ in order to ensure that all wavelets $\psi_{s,\xi}(t) = w(s)\psi\left(\frac{t - \xi}{s}\right)$ at every scale, s , have the same energy, and according to Eq. (16),

$$\int_0^{\infty} |\psi_{s,\xi}(t)|^2 dt = \int_0^{\infty} \left| \frac{1}{\sqrt{s}} \psi\left(\frac{t - \xi}{s}\right) \right|^2 dt = \|\psi_{s,\xi}(t)\|_2 = \text{constant} \quad \forall s. \quad (18)$$

The same energy requirement among all the daughter wavelets $\psi_{s,\xi}(t)$ is the default setting in the MATLAB (2017) Wavelet Toolbox; however, the same energy requirement is, by all means, not a restriction. Clearly, there are applications where it is more appropriate that all daughter wavelets, $\psi_{s,\xi}(t)$, at every scale, s , enclose the same area (not same energy) and, in this case, $w(s) = \frac{1}{s}$; therefore (Vassiliou and Makris 2011),

$$\int_0^{\infty} |\psi_{s,\xi}(t)| dt = \int_0^{\infty} \left| \frac{1}{s} \psi\left(\frac{t - \xi}{s}\right) \right| dt = \|\psi_{s,\xi}(t)\|_1 = \text{constant} \quad \forall s. \quad (19)$$

On the other hand, there may be applications where it is more appropriate that all daughter wavelets

have merely the same maximum value and, in this case, $w(s) = 1$ and

$$\|\psi_{s,\xi}(t)\|_{\infty} = \text{constant} \quad \forall s. \quad (20)$$

The need to include four parameters in a mathematical expression of a simple wavelike function that is a good candidate to express the coherent component of a recorded ground motion was first recognized and addressed by [Mavroeidis and Papageorgiou \(2003\)](#) with the velocity pulse expressed by Eq. (10). Clearly the wavelike signal given by Eq. (10) does not always have a zero mean; therefore, it cannot be a wavelet within the context of wavelet transform. Nevertheless, the time derivative of the elementary velocity signal given by Eq. (10) after setting $t_0 = 0$ is:

$$\frac{dv(t)}{dt} = -\frac{\pi f_p}{\gamma} \left\{ \sin\left(\frac{2\pi f_p t}{\gamma}\right) \cos(2\pi f_p t + \phi) + \gamma \sin(2\pi f_p t + \phi) \left[1 + \cos\left(\frac{2\pi f_p t}{\gamma}\right) \right] \right\}, \quad (21)$$

$$-\frac{\gamma}{2f_p} \leq t \leq \frac{\gamma}{2f_p}$$

which is, by construction, a zero-mean signal; and was coined by [Vassiliou and Makris \(2011\)](#) as the *Mavroeidis and Papageorgiou (M&P) wavelet*. After replacing the oscillatory frequency, f_p , with the inverse of the scale parameter, $\frac{1}{s}$ the M&P wavelet expressed in Eq. (21) is defined as

$$\psi\left(\frac{t-\xi}{s}, \gamma, \phi\right) = \left\{ \sin\left[\frac{2\pi}{s\gamma}(t-\xi)\right] \cos\left[\frac{2\pi}{s}(t-\xi) + \phi\right] \right\} \quad (22)$$

$$+ \gamma \sin\left[\frac{2\pi}{s}(t-\xi) + \phi\right] \left\{ 1 + \cos\left[\frac{2\pi}{s\gamma}(t-\xi)\right] \right\}, \quad \xi - \frac{\gamma}{2f_p} \leq t \leq \xi + \frac{\gamma}{2f_p}$$

after removing the multiplication factor, $\frac{\pi f_p}{\gamma}$, appearing in Eq. (21). In the expression for the M&P wavelet given by Eq. (22), the dilation-contraction is controlled with the parameter s while the movement of the wavelet along the time axis is controlled with translation parameter ξ , the same way as is done in the Ricker wavelet given by Eq. (15). The novel attraction in the M&P wavelet given by Eq. (22) is that, in addition to the dilation-contraction and translation $\frac{t-\xi}{s}$, the wavelet can be further manipulated by modulating the phase, ϕ , and the parameter, γ , which controls the oscillatory character (number of half cycles). Accordingly, [Vassiliou and Makris \(2011\)](#) proposed the four-parameter wavelet transform as:

$$C(s, \xi, \gamma, \phi) = w(s, \gamma, \phi) \int_0^{\infty} \ddot{u}_g(t) \psi\left(\frac{t-\xi}{s}, \gamma, \phi\right) dt. \quad (23)$$

The inner product, given by Eq. (23), is performed repeatedly by scanning not only at all times, ξ , and all scales, s , but also by scanning various phases, $\phi = \{0, \pi/4, \pi/2, 3\pi/4, 2\pi\}$, and various values of the oscillatory nature of the signal $\gamma = \{1, 1.5, 2, 2.5, 3\}$. When needed, more values of ϕ and γ may be scanned. The quantity $w(s, \gamma, \phi)$ outside the integral is a weighting function, which is adjusted according to the application. The values of $s = S$, $\xi = \Xi$, $\gamma = \Gamma$, $\phi = \Phi$, for which the coefficient $C(s, \xi, \gamma, \phi) = C(S, \Xi, \Gamma, \Phi)$ reaches its maximum value, offer the scale, time location, phase, and number of half cycles of the wavelet $\psi\left(\frac{t-\xi}{s}, \gamma, \phi\right)$ that locally best matches the acceleration record, $\ddot{u}_g(t)$. The multiplication coefficient, $\lambda(S, \Xi, \Gamma, \Phi)$, which dictates how much the best-matching generalized wavelet $w(S, \Gamma, \Phi) \cdot \psi_{S, \Xi, \Gamma, \Phi}(t)$ needs to be amplified to best approximate the energetic acceleration pulse, is (Vassiliou and Makris 2011)

$$\lambda(S, \Xi, \Gamma, \Phi) = \frac{C(S, \Xi, \Gamma, \Phi)}{w^2(S, \Gamma, \Phi) \cdot S \cdot E(\Gamma, \Phi)}. \quad (24)$$

For instance, the mathematical wavelets that best match the acceleration records shown in Figs. 1 and 2 have been extracted with the extended wavelet transform defined by Eq. (23).

5 Pulse-Period – Moment-Magnitude Relations with Engineering Significance

The initial motivation of Bertero *et al.* (1976, 1978) to divert the attention of engineers to coherent acceleration pulses and the ongoing interest in identifying and characterizing them are primarily motivated from the need to estimate inelastic deformation demands on structures like those plotted in Fig. 3. Clearly, the more a ground motion is pulse-like, the more the results from self-similar master curves like the one presented by Makris and Psychogios (2006) and Karavasilis *et al.* (2010) become dependable. Accordingly, some indicator is needed to indicate to what extent a recorded ground motion is pulse-like. Efforts to classify ground motions have been presented in the past. Baker (2007), after a preliminary visual classification of the velocity records, proceeds by proposing a pulse indicator that is a function of a *PGV* ratio and an energy ratio. Clearly, both the *PGV* ratio and the energy ratio involve information solely from the velocity time history, and therefore Baker's pulse indicator does not have the ability to identify shorter duration pulses that occasionally govern to a great extent the response of structures as shown in Fig. 8.

In view of the engineering significance that emerges when a shorter-duration pulse overrides a long-duration pulse as illustrated in Fig. 8, Vassiliou and Makris (2011) proposed a pulse

indicator (PI)

$$\text{PI} = \frac{1}{2}(e_a + e_v) \quad (25)$$

where

$$e_a = \frac{\int_0^\infty \ddot{u}(t) \cdot \lambda(S, \Xi, \Gamma, \Phi) w(S, \Gamma, \Phi) \psi_{S, \Xi, \Gamma, \Phi}(t) dt}{\int_0^\infty [\ddot{u}(t)]^2 dt} \quad (26)$$

is a scalar measure of the performance of the best matching wavelet, $\lambda(S, \Xi, \Gamma, \Phi) w(S, \Gamma, \Phi)$ to locally match the predominant acceleration pulse and

$$e_v = \frac{\int_0^\infty \dot{u}(t) \cdot v(t) dt}{\int_0^\infty [\dot{u}(t)]^2 dt} \quad (27)$$

where $v(t)$ is the velocity pulse associated with the extracted acceleration pulse $\lambda(S, \Xi, \Gamma, \Phi) \cdot w(S, \Gamma, \Phi) \psi_{S, \Xi, \Gamma, \Phi}(t)$

$$v(t) = \int \lambda(S, \Xi, \Gamma, \Phi) w(S, \Gamma, \Phi) \psi_{S, \Xi, \Gamma, \Phi}(t) dt \quad (28)$$

The matching indices e_a and e_v of all 1260 candidate records with epicentral distance $D \leq 20$ km were computed and each record that exhibited a pulse indicator $\text{PI} = \frac{1}{2}(e_a + e_v) \geq 0.3$ was classified as a pulse-like record [Vassiliou and Makris \(2011\)](#). Accordingly, among the 447 normal fault records with epicentral distance $D \leq 20$ km, 109 records were classified as pulse-like ($\text{PI} \geq 0.3$) with their pulse periods shown in Fig. 10 (top). Similarly, among the 478 reverse fault records with epicentral distance $D \leq 20$ km, 188 records were classified as pulse-like ($\text{PI} \geq 0.3$) with their pulse periods shown in Fig. 10 (center); whereas, among the 335 strike-slip fault records with epicentral distance ≤ 20 km, 125 records were classified as pulse-like ($\text{PI} \geq 0.3$) with their pulse periods shown in Fig. 10 (bottom). For the complete list of the pulse-like ground motions and the characteristics of the extracted pulses, see Tables S1, S2 and S3 in the supplement at the end of this article.

The extracted pulse periods with the extended wavelet transform given by Eq. (23) of the pulse-like records with epicentral distance $D \leq 10$ km are shown in Fig. 10 with diamonds. Similarly, the extracted pulse periods of the pulse-like records with epicentral distance 10 km

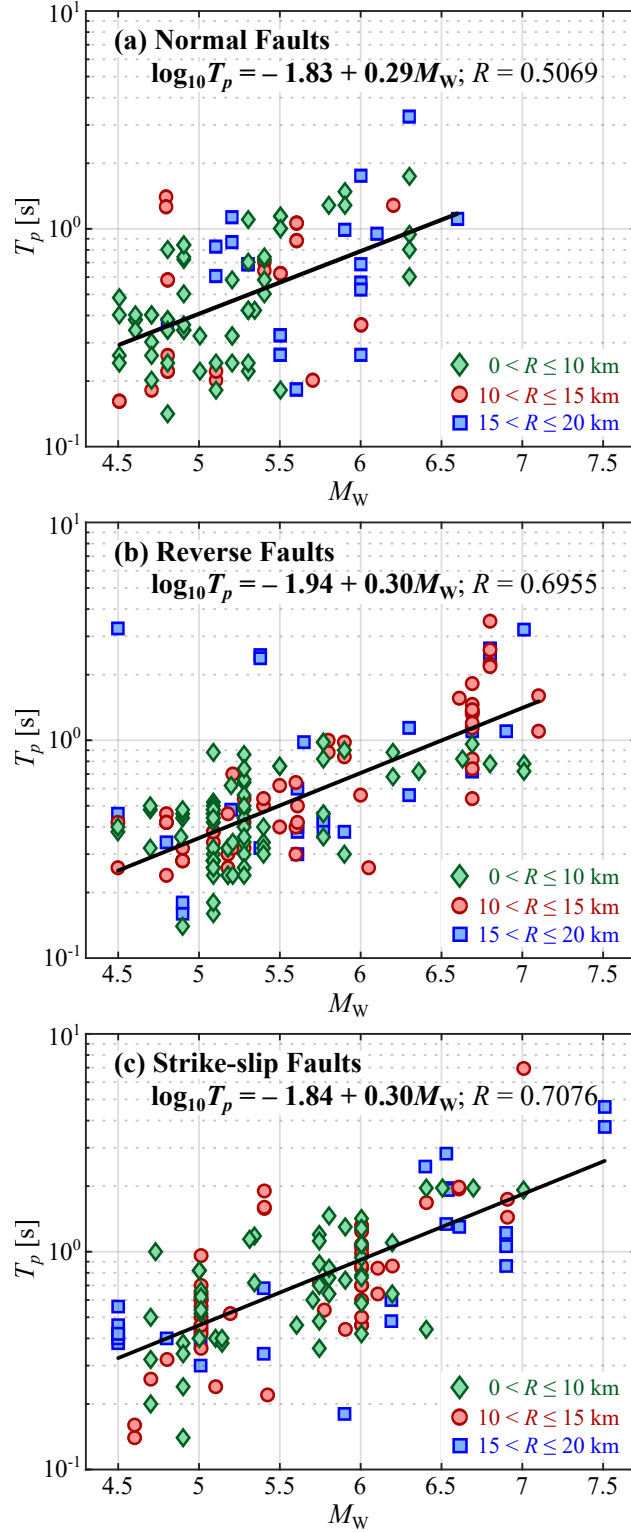


Figure 10: Pulse periods extracted with the extended wavelet transform (Eq. (23)) of the 109 pulse-like records ($PI \geq 0.3$) generated from normal faults (a); the 188 pulse-like records ($PI \geq 0.3$) generated from reverse faults (b); and the 125 pulse-like records ($PI \geq 0.3$) generated from strike-slip faults (c).

$< D \leq 15$ km are shown in Fig. 10 with open circles; whereas, the extracted pulse periods of the pulse-like records with epicentral distance $15 \text{ km} < D \leq 20$ km are shown with open squares.

The straight solid lines in Fig. 10 result from regression analysis of all the extracted data ($D \leq 20$ km) appearing in each subplot and are:

$$\log_{10} T_{p_{\text{NF}}} = -1.83 + 0.29M_W, \quad \text{with} \quad R = 0.5069 \quad (29)$$

for dip-slip normal faults (NF),

$$\log_{10} T_{p_{\text{RF}}} = -1.94 + 0.30M_W, \quad \text{with} \quad R = 0.6955 \quad (30)$$

for dip-slip reverse faults (RF), and

$$\log_{10} T_{p_{\text{SSF}}} = -1.84 + 0.30M_W, \quad \text{with} \quad R = 0.7076 \quad (31)$$

for strike-slip faults (SSF). In Eqs. (29) – (31), R is the correlation coefficient (Weisberg 2005).

The proximity of the coefficients of Eqs. (29) and (31) suggests that the same T_p – M_W equation can be used for normal dip-slip faults and strike-slip faults; whereas, Eq. (30) is recommended for reverse dip-slip faults. Figure 11 plots Eqs. (30) and (31) that have been derived after interrogating with wavelet analysis acceleration pulse-like records against the published T_p – M_W relations presented in Fig. 4 which have been derived by merely matching velocity pulses. Our findings, that emerge from wavelet analysis on acceleration records, confirm past observations by Somerville (1998) and Mavroeidis and Papageorgiou (2003) that for the same moment magnitude, M_W , the pulse periods of ground motions generated from strike-slip faults are on average larger than the pulse periods generated from reverse dip-slip faults. Nevertheless, our proposed T_p – M_W relations expressed by Eqs. (30) and (31) are shown in Fig. 11 with heavy lines manifest a lower slope than the slopes of the T_p – M_W relations plotted by past investigators after matching velocity pulses. As a result, our proposed relations expressed by Eqs. (30) and (31) suggest appreciably shorter pulse periods for ground motions generated by earthquakes with moment magnitude $M_W \geq 6$.

The pulse periods of the individual pulse-like ground motions shown in Fig. 10 that have

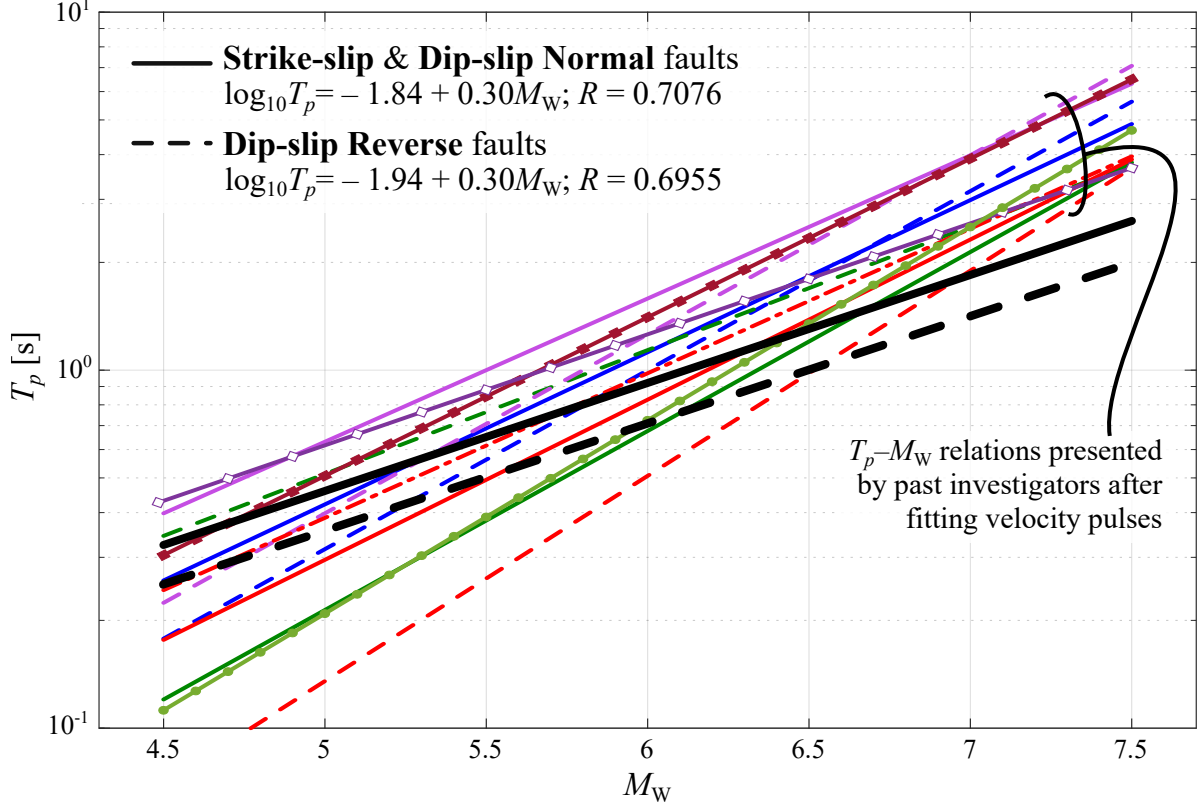


Figure 11: Proposed T_p – M_W relations for pulse-like ground motions with epicentral distance $D \leq 20$ km for strike-slip and normal dip-slip faults (heavy solid line: Eq. (31)) and for reverse dip-slip faults (heavy dashed line: Eq. (30)) extracted with wavelet analysis on the acceleration records.

been extracted with wavelet analysis of the acceleration records are compared with the mean period

$$T_m = \frac{\sum_j C_j^2 \frac{1}{f_j}}{\sum_j C_j^2} \quad \text{for } 0.25 \text{ Hz} \leq f_j \leq 20 \text{ Hz} \quad (32)$$

proposed by Rathje *et al.* (1998). In Eq. (32) f_j are discrete frequencies between 0.25 Hz and 20 Hz; whereas, C_j are the Fourier amplitudes of the Fourier transform of the acceleration record evaluated at frequencies f_j . The horizontal axis (logarithmic scale) of Fig. 12 indicates the computed mean period, T_m , of all the pulse-like ground motions summarized in Fig. 10; whereas, the vertical axis (linear scale) indicates the pulse periods of all the pulse-like ground motions appearing in Fig. 10 which have been extracted with wavelet analysis of the acceleration records. Figure 12 uncovers that the mean period, T_m , offered by Eq. (32) and proposed by Rathje *et al.* (1998) is invariably lower than the pulse periods extracted with wavelet analysis. This is anticipated since Eq. (32)

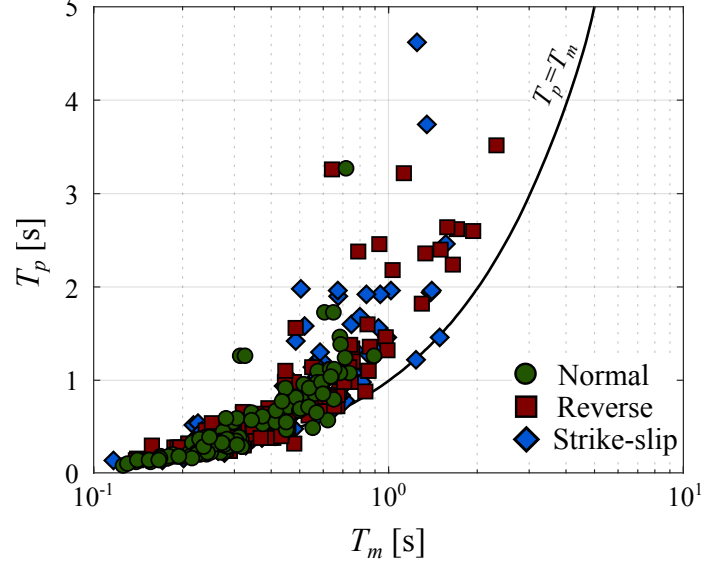


Figure 12: Comparison of the pulse period T_p of all the pulse-like ground motions appearing in Fig. 10 which have been extracted with wavelet analysis on the acceleration records together with the period T_m offered by Eq. (32) (Rathje *et al.* 1998).

factors several high-frequency spikes with periods much lower than the period of the dominant distinguishable pulse extracted with wavelet analysis. Accordingly, for earthquakes with $M_W > 6$ our proposed T_p – M_W relations expressed by Eqs. (30) and (31) offer pulse periods, which are lower than these offered by the T_p – M_W relations proposed by other investigators and summarized in Fig. 4; yet our pulse periods remain larger than the mean periods, T_m , offered by Eq. (32).

Consequently, our proposed wavelet analysis on acceleration pulse-like records and the resulting revised T_p – M_W relations yield objective T_p values allowing for the estimation of dependable peak structural displacements that scale invariantly with $a_p T_p^2$.

6 Conclusions

We have revisited the pulse-period – moment-magnitude (T_p – M_W) relations of pulse-like ground motions generated from near-source earthquakes with epicentral distances $D \leq 20$ km. A total of 1260 ground motions are interrogated with wavelet analysis and the associated extended wavelet transform (Vassiliou and Makris 2011) to identify energetic acceleration pulses (not velocity pulses) and extract their optimal period, T_p , amplitude a_p , phase ϕ , and number of half-sines γ .

The interrogation of acceleration records with wavelet analysis is capable of extracting shorter-

duration distinguishable pulses with engineering significance which override the longer near-source pulses that are not of random character. The pulse-like character of any given record was established with the implementation of a pulse indicator, $PI = \frac{1}{2}(e_a + e_v)$ where e_a and e_v are scalar measures of the performance of the best matching wavelet on the acceleration record and the velocity record.

The extended wavelet transform that was employed in this study identified 109 pulse-like records from normal faults, 188 pulse-like records from reverse faults and 125 pulse-like records from strike-slip faults, all with epicentral distances, $D \leq 20$ km. Regression analysis on the extracted periods concluded that the same T_p - M_W relation can be used for pulse-like ground motions generated either from strike-slip faults or from dip-slip normal faults; whereas, a different T_p - M_W relation is proposed for dip-slip reverse faults.

The study concludes that for the same moment magnitude, M_W , the pulse period of ground motions generated from strike-slip faults are on average larger than these from reverse faults — a result that is in agreement with findings from past investigators. At the same, our wavelet analysis on acceleration records produces T_p - M_W relations with a lower slope than the slopes of the T_p - M_W relations presented by past investigators who concentrated on velocity pulses. As a result, our proposal T_p - M_W relations yield lower T_p value for larger magnitude earthquakes (say $M_W > 6$); yet they remain higher than the mean period, T_m , proposed by Rathje *et al.* (1998). Accordingly, our results allow for the estimation of dependable peak structural displacements that scale invariably with $a_p T_p^2$.

Data and Resources

The earthquake records listed in Tables S1, S2 and S3 in the supplement to this paper were downloaded from:

1. <https://ngawest2.berkeley.edu> (Last accessed April 2021)
2. <http://www.isesd.hi.is> (Last accessed April 2021)

All the computations, numerical analysis, and plotting have been performed with the software MATLAB (2017). <https://www.mathworks.com> (last accessed April 2021).

References

- Addison, P. S. (2002). *The illustrated wavelet transform handbook*. Institute of Physics Handbook, London press.
- Addison, P. S. (2017). *The illustrated wavelet transform handbook: introductory theory and applications in science, engineering, medicine and finance*. CRC press.
- Aki, K. and Richards, P. G. (1980). *Quantitative Seismology: Theory and Methods*. Freeman.
- Alavi, B. and Krawinkler, H. (2000). Consideration of near-fault ground motion effects in seismic design. In *Proceedings of the 12th World Conference on Earthquake Engineering*, page 8.
- Ambraseys, N., Smit, P., Sigbjörnsson, R., Suhadolc, P., and Margaris, B. (2002). Internet-site for European strong-motion data. *European Commission, Research-Directorate General, Environment and Climate Programme*.
- Ancheta, T. D., Darragh, R. B., Stewart, J. P., Seyhan, E., Silva, W. J., Chiou, B. S., Wooddell, K. E., Graves, R. W., Kottke, A. R., Boore, D. M., Kishida, T., and Donahue, J. L. (2013). Peer NGA-West2 database. *Pacific Earthquake Engineering Research Center Berkeley, CA*.
- Baker, J. W. (2007). Quantitative classification of near-fault ground motions using wavelet analysis. *Bulletin of the Seismological Society of America*, 97(5):1486–1501.
- Barenblatt, G. I. (1996). *Scaling, self-similarity, and intermediate asymptotics: dimensional analysis and intermediate asymptotics*. Number 14. Cambridge University Press.
- Bertero, V. V., Anderson, J. C., Krawinkler, H., and Miranda, E. (1991). Design guidelines for ductility and drift limits. *Rep. No. UCB/EERC-91*, 15.
- Bertero, V. V., Herrera, R. A., and Mahin, S. A. (1976). Establishment of design earthquakes—evaluation of present methods. In *Proc., Int. Symp. on Earthquake Structural Engineering*, volume 1, pages 551–580. Univ. of Missouri-Rolla Rolla, Mo.
- Bertero, V. V., Mahin, S. A., and Herrera, R. A. (1978). Aseismic design implications of near-fault san fernando earthquake records. *Earthquake Engineering & Structural Dynamics*, 6(1):31–42.

- Bolt, B. A. (1971). The San Fernando valley, California, earthquake of February 9 1971: Data on seismic hazards. *Bulletin of the Seismological Society of America*, 61(2):501–510.
- Bolt, B. A. (1975). How are magnitude, epicenter, focal depth determined? Degree of accuracy? Describe P and S waves, etc. In *Engineering Aspects of the Lima, Peru Earthquake of October 3, 1974*, pages 74–75. Earthquake Engineering Research Institute.
- Bray, J. D. and Rodriguez-Marek, A. (2004). Characterization of forward-directivity ground motions in the near-fault region. *Soil dynamics and earthquake engineering*, 24(11):815–828.
- FEMA (2000). *NEHRP Recommended Seismic Provisions for New Buildings and Other Structures*.
- FEMA-273 (1997). *NEHRP Guidelines for the Seismic Rehabilitation of Buildings*.
- Fu, Q. and Menun, C. (2004). Seismic-environment-based simulation of near-fault ground motions. In *Proceedings of the 13th World Conference on Earthquake Engineering*.
- Gabor, D. (1946). Theory of communication. Part 1: The analysis of information. *Journal of the Institution of Electrical Engineers-Part III: Radio and Communication Engineering*, 93(26):429–441.
- Hall, J. F., Heaton, T. H., Halling, M. W., and Wald, D. J. (1995). Near-source ground motion and its effects on flexible buildings. *Earthquake Spectra*, 11(4):569–605.
- Housner, G. and Trifunac, M. (1967). Analysis of accelerograms—Parkfield earthquake. *Bulletin of the Seismological Society of America*, 57(6):1193–1220.
- Housner, G. W. and Hudson, D. E. (1958). The Port Hueneme earthquake of March 18, 1957. *Bulletin of the Seismological Society of America*, 48(2):163–168.
- Housner, G. W. and Hudson, D. E. (1959). Applied mechanics-dynamics. vol. ii, princeton, n. j.
- IBC (2000). *2000 International Building Code*.
- Iwan, W. and Chen, X. (1994). Important near-field ground motion data from the Landers earthquake. In *Proceedings of the 10th European Conference on Earthquake Engineering*, volume 1, pages 229–234. AA Balkema Rotterdam, The Netherlands.

- Karavasilis, T. L., Makris, N., Bazeos, N., and Beskos, D. E. (2010). Dimensional response analysis of multistory regular steel MRF subjected to pulselike earthquake ground motions. *Journal of Structural Engineering*, 136(8):921–932.
- Krawinkler, H. and Alavi, B. (1998). Development of improved design procedures for near-fault ground motions. In *SMIP98 Seminar on Utilization of Strong-Motion Data*, pages 21–41.
- Langhaar, H. L. (1951). *Dimensional analysis and theory of models*. Wiley.
- Loh, C.-H., Lee, Z.-K., Wu, T.-C., and Peng, S.-Y. (2000). Ground motion characteristics of the Chi-Chi earthquake of 21 September 1999. *Earthquake Engineering & Structural Dynamics*, 29(6):867–897.
- Ma, K.-F., Mori, J., Lee, S.-J., and Yu, S. (2001). Spatial and temporal distribution of slip for the 1999 Chi-Chi, Taiwan, earthquake. *Bulletin of the Seismological Society of America*, 91(5):1069–1087.
- Makris, N. (1997). Rigidity–plasticity–viscosity: Can electrorheological dampers protect base-isolated structures from near-source ground motions? *Earthquake Engineering & Structural Dynamics*, 26(5):571–591.
- Makris, N. and Black, C. J. (2004a). Dimensional analysis of rigid-plastic and elastoplastic structures under pulse-type excitations. *Journal of Engineering Mechanics*, 130(9):1006–1018.
- Makris, N. and Black, C. J. (2004b). Dimensional analysis of bilinear oscillators under pulse-type excitations. *Journal of Engineering Mechanics*, 130(9):1019–1031.
- Makris, N. and Chang, S.-P. (2000). Response of damped oscillators to cycloidal pulses. *Journal of Engineering Mechanics*, 126(2):123–131.
- Makris, N. and Psychogios, T. (2006). Dimensional response analysis of yielding structures with first-mode dominated response. *Earthquake Engineering & Structural Dynamics*, 35(10):1203–1224.
- MATLAB (2017). *Version 9.2 (R2017a)*. The MathWorks Inc., Natick, Massachusetts.

- Mavroeidis, G. P. and Papageorgiou, A. S. (2003). A mathematical representation of near-fault ground motions. *Bulletin of the Seismological Society of America*, 93(3):1099–1131.
- Newmark, N. M. (1965). Effects of earthquakes on dams and embankments. *Geotechnique*, 15(2):139–160.
- Rathje, E. M., Abrahamson, N. A., and Bray, J. D. (1998). Simplified frequency content estimates of earthquake ground motions. *Journal of Geotechnical and Geoenvironmental Engineering*, 124(2):150–159.
- Ricker, N. (1943). Further developments in the wavelet theory of seismogram structure. *Bulletin of the Seismological Society of America*, 33(3):197–228.
- Ricker, N. (1944). Wavelet functions and their polynomials. *Geophysics*, 9(3):314–323.
- Rodriguez-Marek, A. (2000). *Near-fault seismic site response*. PhD thesis, University of California, Berkeley.
- Sekiguchi, H. and Iwata, T. (2002). Rupture process of the 1999 Kocaeli, Turkey, earthquake estimated from strong-motion waveforms. *Bulletin of the Seismological Society of America*, 92(1):300–311.
- Somerville, P. and Graves, R. (1993). Conditions that give rise to unusually large long period ground motions. *The structural design of tall buildings*, 2(3):211–232.
- Somerville, P. G. (1998). Development of an improved representation of near fault ground motions. In *SMIP98 Seminar on Utilization of Strong-Motion Data*, volume 15, page 1998.
- Somerville, P. G. (2003). Magnitude scaling of the near fault rupture directivity pulse. *Physics of the earth and planetary interiors*, 137(1-4):201–212.
- UBC (1997). *1997 Uniform Building Code*.
- Vassiliou, M. F. and Makris, N. (2011). Estimating time scales and length scales in pulslike earthquake acceleration records with wavelet analysis. *Bulletin of the Seismological Society of America*, 101(2):596–618.

- Veletsos, A. S. and Newmark, N. M. (1960). Effect of inelastic behavior on the response of simple systems to earthquake motions. In *Proceedings of the 2nd World Conference on Earthquake Engineering*, pages 895–912.
- Veletsos, A. S., Newmark, N. M., and Chelapati, C. (1965). Deformation spectra for elastic and elastoplastic systems subjected to ground shock and earthquake motions. In *Proceedings of the 3rd World Conference on Earthquake Engineering*, volume 2, pages 663–682.
- Wang, W.-H., Chang, S.-H., and Chen, C.-H. (2001). Fault slip inverted from surface displacements during the 1999 Chi-Chi, Taiwan, earthquake. *Bulletin of the Seismological Society of America*, 91(5):1167–1181.
- Weisberg, S. (2005). *Applied linear regression*, volume 528. John Wiley & Sons.

Supplement

Tables of Strong Ground Motions

The list of pulse-like ground motions and their pulse characteristics are presented in Tables [S1](#), [S2](#) and [S3](#). For the database of pulses, records of strong ground motions from the Next Generation Attenuation (NGA) ([Ancheta et al. 2013](#)) database and the European Strong Motion Database ([Ambraseys et al. 2002](#)) with the following characteristics were used:

- Moment magnitude, $M_w \geq 4.5$, and
- Epicentral distance, $D \leq 20$ km

The records were categorized based on their fault mechanism, as provided by the descriptions of the NGA and the European Strong Motion databases.

D [km] : epicentral distance

M_w : moment magnitude

PI : pulse indicator

e_a : matching index for the extracted acceleration pulse

e_v : matching index for the obtained (from the acceleration pulse) velocity pulse

a_p [g] : amplitude of the acceleration pulse

v_p [m/s] : corresponding velocity amplitude of the elementary wavelet

t_0 [s] : time instance when the pulse starts

T_p [s] : period of the acceleration pulse

ϕ [rad] : phase of the elementary wavelet

γ : parameter that controls the oscillatory character of the elementary wavelet

S_a [g] : pseudoacceleration of an elastic SDoF oscillator

The pulses that result in larger pseudoaccelerations of the two elastic SDoF oscillators with $T_0 = 0.5$ and 2.5 s than those of recorded ground motions are shown in **bold** font

Table S1: Near-source, pulse-like ground motions from dip-slip normal faults and the parameters of the extracted pulses.

Legend	
D	Epicentral distance
M_W	moment magnitude
PI	pulse indicator
e_a	matching index for the extracted acceleration pulse
e_v	matching index for the obtained velocity pulse
a_p	amplitude of the acceleration pulse
v_p	corresponding velocity amplitude of the elementary wavelet
t_0	time instance when the acceleration pulse starts
T_p	period of the pulse
φ	phase of the elementary wavelet
γ	parameter that controls the oscillatory character of the elementary wavelet
S_a	pseudoacceleration of an elastic SDoF oscillator

The pulses that result in larger pseudoaccelerations of the two elastic SDoF oscillators with $T_0=0.5$ and 2.5s than those of recorded ground motions are shown in **bold** font

Earthquake Records from
Dip-Slip Normal Faults

No.	EQ name	Year	Station name	D [km]	M_W	PI	e_a	e_v	a_p [g]	v_p [m/s]	t_0 [s]	T_p [s]	φ [rad]	γ	$S_{a,p}$ [g] $T_0=0.5s$	$S_{a,p}$ [g] $T_0=2.5s$
1	Aigion (aftershock)	1995	ST1330/x	18.0	5.3	0.59	0.48	0.69	0.01	0.01	7.57	0.68	3.14	1.50	0.02	0.00
2	Alkion	1981	ST122/y	19.0	6.6	0.30	0.31	0.29	0.16	0.25	6.60	1.10	2.36	1.00	0.40	0.04
3	Almiros (aftershock)	1980	ST1300/y	10.0	4.8	0.31	0.28	0.33	0.03	0.04	2.26	0.80	1.57	2.00	0.09	0.00
4	Ano Liosia	1999	ST1100/x	16.0	6	0.39	0.25	0.52	0.14	0.13	4.12	0.68	1.57	2.00	0.43	0.01
5		1999	ST1100/y	16.0	6	0.34	0.46	0.22	0.31	0.13	3.97	0.26	2.36	2.50	0.16	0.00
6		1999	ST1101/x	17.0	6	0.36	0.33	0.40	0.09	0.09	3.74	0.56	0.00	1.50	0.24	0.01
7		1999	ST1141/x	19.0	6	0.42	0.23	0.62	0.04	0.09	9.44	1.74	2.36	1.00	0.05	0.02
8		1999	ST1257/y	18.0	6	0.36	0.49	0.24	0.09	0.07	9.46	0.52	1.57	2.00	0.24	0.01
9		1999	ST1258/x	14.0	6	0.33	0.40	0.27	0.23	0.11	9.01	0.36	1.57	2.00	0.26	0.01
10		1999	ST1259/y	14.0	6	0.30	0.30	0.30	0.29	0.16	6.70	0.36	2.36	2.00	0.33	0.01
11	Borah Peak, ID-02	1983	BOR/000	18.0	5.1	0.34	0.40	0.27	0.06	0.05	6.58	0.60	2.36	3.00	0.21	0.00
12		1983	BOR/090	18.0	5.1	0.62	0.59	0.65	0.07	0.09	5.28	0.82	2.36	1.50	0.20	0.01
13	Campano Lucano (aftershock 3), Italy	1980	Contrada Fiumicella-Teora/000	9.9	4.5	0.45	0.49	0.41	0.08	0.03	1.42	0.24	1.57	2.00	0.03	0.00
14		1980	Contrada Fiumicella-Teora/090	9.9	4.5	0.50	0.39	0.60	0.05	0.03	1.42	0.48	0.79	1.00	0.06	0.00
15	Campano Lucano (aftershock 4), Italy	1980	Contrada Fiumicella-Teora/000	6.1	4.6	0.44	0.42	0.45	0.20	0.08	1.34	0.38	1.57	1.00	0.15	0.00
16		1980	Contrada Fiumicella-Teora/090	6.1	4.6	0.41	0.34	0.47	0.11	0.07	1.63	0.38	0.79	3.00	0.19	0.00
17	Campano Lucano (aftershock)	1981	ST115/y	5.0	5.2	0.34	0.40	0.29	0.17	0.06	2.58	0.24	0.79	2.50	0.07	0.00
18		1981	ST111/y	8.0	5.2	0.49	0.42	0.56	0.09	0.08	0.94	0.58	0.00	3.00	0.34	0.01
19	Drama	1985	ST1305/x	19.0	5.2	0.37	0.27	0.46	0.03	0.04	2.72	0.86	2.36	2.00	0.07	0.01
20		1985	ST1305/y	19.0	5.2	0.55	0.33	0.78	0.03	0.06	1.83	1.12	2.36	2.50	0.04	0.01
21	Dursunbey, Turkey	1979	Dursunbey/L	6.0	5.34	0.39	0.34	0.44	0.12	0.09	1.31	0.42	0.00	3.00	0.29	0.00
22	Gulf of Corinth	1988	ST1319/x	19.0	4.5	0.38	0.51	0.25	0.06	0.02	1.25	0.26	2.36	1.50	0.03	0.00
23		1993	ST178/y	10.0	5.3	0.52	0.45	0.59	0.08	0.09	1.61	0.70	0.00	1.50	0.23	0.01
24	Irpinia, Italy-02	1980	Calitri/000	12.0	6.2	0.43	0.36	0.50	0.12	0.22	7.67	1.28	1.57	3.00	0.15	0.05
25	Irpinia, Italy-03	1981	Cairano 1/CR1000	4.7	4.7	0.30	0.23	0.37	0.09	0.06	2.35	0.40	2.36	2.50	0.16	0.00
26		1981	Cairano 2/CR2090	4.9	4.7	0.36	0.41	0.30	0.16	0.06	2.49	0.26	0.79	2.50	0.08	0.00
27	Izmir, Turkey	1977	Izmir/L	2.3	5.3	0.75	0.78	0.73	0.37	0.12	0.52	0.22	1.57	3.00	0.11	0.00
28		1977	Izmir/T	2.3	5.3	0.56	0.61	0.52	0.13	0.05	0.77	0.24	0.00	3.00	0.05	0.00
29	Kalamata	1986	ST164/x	10.0	5.9	0.41	0.22	0.59	0.12	0.27	3.86	1.48	0.79	2.00	0.14	0.08
30	Kalamata (aftershock)	1986	ST164/x	1.0	4.9	0.73	0.62	0.83	0.30	0.26	2.51	0.84	1.57	1.00	0.80	0.03
31		1986	ST163/x	3.0	4.9	0.67	0.65	0.68	0.25	0.26	2.58	0.72	0.79	1.00	0.56	0.03

No.	EQ name	Year	Station name	D [km]	M_W	PI	e_a	e_v	a_p [g]	v_p [m/s]	t_0 [s]	T_p [s]	ϕ [rad]	γ	$S_{a,p}$ [g] $T_0=0.5s$	$S_{a,p}$ [g] $T_0=2.5s$
79	Umbria Marche (aftershock 12), Italy	1997	Sellano Ovest/090	2.2	4.6	0.73	0.63	0.82	0.04	0.02	16.50	0.34	2.36	3.00	0.04	0.00
80	Umbria Marche (aftershock 13), Italy	1997	Sellano Ovest/000	7.3	4.9	0.37	0.40	0.33	0.04	0.02	16.35	0.34	0.00	3.00	0.05	0.00
81		1997	Sellano Ovest/090	7.3	4.9	0.34	0.32	0.36	0.03	0.02	17.09	0.36	0.00	2.50	0.05	0.00
82	Umbria Marche (aftershock 15), Italy	1998	Sellano Ovest/000	8.7	5	0.48	0.53	0.42	0.03	0.01	17.31	0.22	1.57	1.00	0.01	0.00
83		1998	Sellano Ovest/090	8.7	5	0.43	0.38	0.48	0.03	0.01	17.33	0.32	0.79	1.00	0.01	0.00
84	Umbria Marche (aftershock 17), Italy	1998	Nocera Umbra-Biscontini/090	10.9	5.1	0.58	0.53	0.62	0.25	0.09	6.93	0.22	0.79	2.50	0.08	0.00
85	Umbria Marche (aftershock 18), Italy	1998	Nocera Umbra-Biscontini/090	11.5	4.8	0.75	0.70	0.81	0.17	0.06	5.60	0.22	3.14	3.00	0.05	0.00
86	Umbria Marche (aftershock 2), Italy	1997	Colfiorito/000	13.0	5.6	0.35	0.28	0.41	0.05	0.07	4.61	0.88	0.00	3.00	0.09	0.01
87		1997	Colfiorito/270	13.0	5.6	0.34	0.24	0.44	0.04	0.06	5.37	1.06	1.57	3.00	0.05	0.01
88	Umbria Marche (aftershock 3), Italy	1997	Colfiorito-Casermette/270	4.4	5.3	0.41	0.30	0.52	0.13	0.09	12.90	0.42	0.00	3.00	0.30	0.00
89	Umbria Marche (aftershock)	1997	ST269/x	7.0	4.9	0.36	0.39	0.32	0.04	0.02	16.44	0.34	3.14	3.00	0.05	0.00
90		1997	ST269/y	7.0	4.9	0.31	0.30	0.31	0.03	0.02	17.21	0.34	0.79	3.00	0.04	0.00
91		1997	ST221/x	7.0	5.3	0.36	0.27	0.44	0.05	0.08	2.56	1.10	2.36	3.00	0.06	0.01
92		1997	ST236/y	5.0	5.3	0.40	0.28	0.52	0.13	0.09	12.98	0.42	0.00	3.00	0.30	0.00
93		1997	ST221/x	7.0	5.5	0.56	0.38	0.74	0.07	0.12	2.58	1.14	2.36	3.00	0.09	0.02
94		1997	ST221/y	7.0	5.5	0.51	0.35	0.67	0.06	0.10	3.26	1.00	2.36	3.00	0.09	0.01
95		1997	ST232/y	15.0	5.5	0.39	0.26	0.53	0.10	0.07	2.66	0.62	1.57	1.50	0.25	0.01
96		1997	ST238/x	20.0	5.5	0.34	0.39	0.29	0.09	0.05	10.85	0.32	0.00	3.00	0.08	0.00
97		1997	ST238/y	20.0	5.5	0.59	0.61	0.56	0.19	0.07	10.95	0.26	1.57	3.00	0.09	0.00
98		1997	ST86/y	20.0	5.6	0.44	0.37	0.50	0.10	0.11	2.96	0.88	1.57	1.50	0.25	0.01
99		1997	ST221/x	13.0	5.6	0.33	0.27	0.38	0.05	0.07	4.70	0.88	0.00	3.00	0.09	0.01
100		1997	ST221/y	13.0	5.6	0.32	0.23	0.41	0.04	0.06	5.46	1.06	1.57	3.00	0.05	0.01
101		1998	ST235/y	11.0	4.8	0.74	0.69	0.80	0.17	0.06	5.68	0.22	0.00	3.00	0.05	0.00
102		1998	ST3177/x	10.0	4.8	0.38	0.37	0.38	0.19	0.04	9.43	0.14	1.57	3.00	0.02	0.00
103		1998	ST235/y	11.0	5.1	0.54	0.53	0.56	0.25	0.07	7.04	0.20	1.57	3.00	0.06	0.00
104		1998	ST3177/x	10.0	5.1	0.51	0.46	0.56	0.39	0.11	8.59	0.18	2.36	3.00	0.07	0.00
105		1998	ST3177/y	10.0	5.1	0.45	0.40	0.51	0.24	0.09	8.63	0.24	0.79	2.00	0.09	0.00
106	Umbria Marche (foreshock), Italy	1997	Nocera Umbra/NCR000	13.2	5.7	0.34	0.32	0.36	0.46	0.15	1.12	0.20	3.14	2.50	0.13	0.00
107	Umbria-03, Italy	1984	Nocera Umbra/NCR000	19.2	5.6	0.40	0.41	0.39	0.21	0.06	4.37	0.18	1.57	3.00	0.04	0.00
108	Valnerina	1979	ST225/y	5.0	5.8	0.39	0.15	0.62	0.07	0.14	3.10	1.28	0.79	1.00	0.16	0.02
109	Veroia, Greece	1984	Edessa (bsmt)/WE	18.9	5.3	0.43	0.42	0.45	0.05	0.05	5.04	0.68	0.79	3.00	0.15	0.00

Table S2: Near-source, pulse-like ground motions from dip-slip reverse faults and the parameters of the extracted pulses.

Legend	
D	Epicentral distance
M_W	moment magnitude
PI	pulse indicator
e_a	matching index for the extracted acceleration pulse
e_v	matching index for the obtained velocity pulse
a_p	amplitude of the acceleration pulse
v_p	corresponding velocity amplitude of the elementary wavelet
t_0	time instance when the acceleration pulse starts
T_p	period of the pulse
φ	phase of the elementary wavelet
γ	parameter that controls the oscillatory character of the elementary wavelet
S_a	pseudoacceleration of an elastic SDoF oscillator

The pulses that result in larger pseudoaccelerations of the two elastic SDoF oscillators with $T_0=0.5$ and 2.5s than those of recorded ground motions are shown in **bold font**

Earthquake Records from
Dip-Slip Reverse Faults

No.	EQ name	Year	Station name	D [km]	M_W	PI	e_a	e_v	a_p [g]	v_p [m/s]	t_0 [s]	T_p [s]	φ [rad]	γ	$S_{a,p}$ [g] $T_0=0.5s$	$S_{a,p}$ [g] $T_0=2.5s$
1	Cape Mendocino	1992	Bunker Hill FAA/BNH270	19.7	7.0	0.49	0.32	0.65	0.11	0.65	4.43	3.22	3.14	1.00	0.13	0.26
2		1992	Petrolia/PET000	4.5	7.0	0.35	0.32	0.39	0.39	0.47	3.52	0.78	2.36	3.00	0.89	0.05
3		1992	Petrolia/PET090	4.5	7.0	0.36	0.45	0.27	0.55	0.62	3.38	0.72	2.36	2.50	1.65	0.06
4	Chi-Chi, Taiwan-02	1999	TCU074/E	5.5	5.9	0.52	0.39	0.66	0.12	0.15	13.59	0.90	1.57	3.00	0.19	0.02
5		1999	TCU079/E	16.2	5.9	0.52	0.53	0.50	0.41	0.16	14.35	0.38	1.57	1.00	0.30	0.01
6		1999	TCU084/E	12.9	5.9	0.39	0.37	0.41	0.09	0.13	15.98	0.98	2.36	1.50	0.19	0.02
7		1999	TCU084/N	12.9	5.9	0.33	0.32	0.35	0.08	0.10	15.93	0.84	2.36	1.50	0.22	0.01
8	Chi-Chi, Taiwan-03	1999	TCU084/E	9.6	6.2	0.44	0.51	0.37	0.16	0.20	24.61	0.88	1.57	3.00	0.28	0.03
9	Chi-Chi, Taiwan-06	1999	TCU078/E	17.9	6.3	0.33	0.24	0.43	0.17	0.34	25.87	1.14	0.00	1.00	0.46	0.05
10		1999	TCU078/N	17.9	6.3	0.31	0.32	0.31	0.37	0.30	25.46	0.56	0.79	1.00	0.62	0.03
11	Chuetsu-oki	2007	Kashiwazaki City Center/EW	19.5	6.8	0.61	0.46	0.76	0.27	1.08	25.45	2.40	0.00	3.00	0.29	0.89
12		2007	Kashiwazaki City Center/NS	19.5	6.8	0.72	0.56	0.87	0.26	1.04	25.61	2.62	0.79	3.00	0.27	0.92
13		2007	Kariwa/EW	13.3	6.8	0.64	0.55	0.73	0.29	1.17	24.38	2.60	2.36	3.00	0.30	1.02
14		2007	Kariwa/NS	13.3	6.8	0.55	0.42	0.68	0.29	1.50	25.79	3.52	1.57	3.00	0.30	0.86
15		2007	Tamati Yone Izumozaki/NS	8.2	6.8	0.32	0.24	0.40	0.39	0.50	25.07	0.78	0.00	3.00	0.97	0.05
16		2007	Kashiwazaki NPP, Service Hall Array/SG01EW	13.6	6.8	0.54	0.46	0.62	0.34	1.18	34.77	2.24	0.79	3.00	0.36	0.91
17		2007	Kashiwazaki NPP, Service Hall Array/SG01NS	13.6	6.8	0.34	0.25	0.43	0.26	0.83	39.11	2.18	0.79	1.00	0.32	0.28
18		2007	NIG018/EW	19.2	6.8	0.59	0.41	0.78	0.24	0.87	22.26	2.36	2.36	3.00	0.25	0.70
19		2007	NIG018/NS	19.2	6.8	0.68	0.50	0.87	0.32	1.31	22.70	2.64	0.79	3.00	0.33	1.15
20	Coalinga-01	1983	Pleasant Valley P.P. - yard/PVY045	10.0	6.4	0.30	0.31	0.30	0.53	0.52	7.27	0.72	1.57	2.00	1.59	0.06
21	Coalinga-02	1983	Anticline Ridge - Palmer Ave/CPL000	4.0	5.1	0.65	0.57	0.73	0.21	0.10	2.32	0.46	1.57	1.00	0.22	0.01
22		1983	Anticline Ridge - Palmer Ave/CPL090	4.0	5.1	0.63	0.47	0.78	0.12	0.08	2.60	0.42	0.79	3.00	0.27	0.00
23		1983	Anticline Ridge Free-Field/ATC270	3.4	5.1	0.65	0.67	0.64	0.42	0.17	2.63	0.26	0.79	3.00	0.21	0.00
24		1983	Anticline Ridge Free-Field/ATC360	3.4	5.1	0.79	0.75	0.83	0.49	0.21	2.55	0.28	0.79	2.50	0.29	0.01
25		1983	Anticline Ridge Pad/ATP270	3.4	5.1	0.73	0.74	0.72	0.49	0.20	2.61	0.26	0.79	3.00	0.24	0.01
26		1983	Anticline Ridge Pad/ATP360	3.4	5.1	0.79	0.80	0.79	0.42	0.18	2.53	0.28	0.79	3.00	0.25	0.01
27		1983	Burnett Construction/BNT270	13.1	5.1	0.44	0.40	0.47	0.06	0.04	3.59	0.42	2.36	3.00	0.13	0.00
28		1983	Burnett Construction/BNT360	13.1	5.1	0.31	0.32	0.31	0.08	0.04	3.24	0.34	0.79	1.00	0.05	0.00
29		1983	Coalinga-14th & Elm (Old CHP)/CHP000	11.6	5.1	0.55	0.53	0.56	0.10	0.05	3.16	0.44	1.57	1.00	0.10	0.00
30		1983	Coalinga-14th & Elm (Old CHP)/CHP090	11.6	5.1	0.62	0.66	0.57	0.10	0.06	3.27	0.38	2.36	2.00	0.13	0.00
31		1983	Harris Ranch - Hdqtrs (temp)/XCH000	13.1	5.1	0.33	0.47	0.18	0.07	0.03	4.36	0.24	3.14	2.50	0.03	0.00

No.	EQ name	Year	Station name	D [km]	M _w	PI	e _a	e _v	a _p [g]	v _p [m/s]	t ₀ [s]	T _p [s]	φ [rad]	γ	S _{a,p} [g] T ₀ =0.5s	S _{a,p} [g] T ₀ =2.5s
32	Coalinga-02	1983	Harris Ranch - Hdqtrs (temp)/XCH090	13.1	5.1	0.51	0.61	0.40	0.11	0.07	4.35	0.38	0.00	1.00	0.10	0.00
33		1983	LLN (temp)/LLN000	5.1	5.1	0.66	0.66	0.66	0.12	0.06	4.69	0.48	1.57	1.00	0.14	0.00
34		1983	Oil City/OLC270	5.8	5.1	0.54	0.53	0.56	0.17	0.07	2.63	0.28	1.57	3.00	0.10	0.00
35		1983	Oil City/OLC360	5.8	5.1	0.37	0.48	0.25	0.32	0.08	2.79	0.16	0.79	3.00	0.04	0.00
36		1983	Oil Fields - Skunk Hollow/COL090	4.0	5.1	0.47	0.36	0.58	0.27	0.08	2.46	0.30	1.57	1.00	0.11	0.00
37		1983	Oil Fields - Skunk Hollow/COL000	4.0	5.1	0.51	0.39	0.62	0.20	0.09	2.66	0.28	2.36	3.00	0.12	0.00
38		1983	Oil Fields Fire Station/OLP270	1.4	5.1	0.38	0.42	0.34	0.20	0.07	2.29	0.24	0.79	1.00	0.06	0.00
39		1983	Palmer Ave/PLM270	4.2	5.1	0.34	0.44	0.24	0.22	0.06	2.48	0.18	2.36	1.50	0.04	0.00
40		1983	Palmer Ave/PLM360	4.2	5.1	0.45	0.52	0.38	0.23	0.11	2.49	0.26	0.00	1.00	0.10	0.00
41		1983	Pleasant Valley P.P. - yard/PVY045	8.2	5.1	0.69	0.52	0.87	0.08	0.10	3.26	0.88	0.79	1.00	0.20	0.01
42		1983	Pleasant Valley P.P. - yard/PVY135	8.2	5.1	0.68	0.68	0.69	0.20	0.10	3.34	0.32	0.79	1.50	0.15	0.01
43		1983	SGT (temp)/SGT350	7.4	5.1	0.48	0.41	0.56	0.16	0.07	5.11	0.28	2.36	3.00	0.10	0.00
44		1983	SUB (temp)/SUB000	8.1	5.1	0.52	0.49	0.54	0.10	0.07	5.13	0.46	0.79	1.00	0.12	0.01
45		1983	SUB (temp)/SUB090	8.1	5.1	0.62	0.67	0.58	0.20	0.09	5.30	0.44	1.57	1.00	0.20	0.01
46		1983	Skunk Hollow/SKH270	3.3	5.1	0.52	0.55	0.49	0.11	0.05	2.62	0.28	2.36	3.00	0.07	0.00
47		1983	Skunk Hollow/SKH360	3.3	5.1	0.55	0.64	0.46	0.11	0.04	2.43	0.26	2.36	1.50	0.05	0.00
48		1983	TRA (temp)/TRA000	9.0	5.1	0.58	0.57	0.60	0.12	0.10	5.45	0.52	2.36	1.50	0.26	0.01
49		1983	TRA (temp)/TRA090	9.0	5.1	0.45	0.52	0.39	0.09	0.07	5.45	0.50	2.36	1.50	0.18	0.00
50		1983	VEW (temp)/VEW005	4.1	5.1	0.65	0.60	0.70	0.10	0.06	4.62	0.48	1.57	1.50	0.17	0.00
51		1983	VEW (temp)/VEW095	4.1	5.1	0.72	0.67	0.77	0.11	0.08	4.74	0.44	2.36	2.00	0.22	0.00
52		Coalinga-03	1983	Burnett Construction/BNT360	15.6	5.4	0.30	0.48	0.11	0.19	0.09	2.29	0.32	2.36	2.00	0.16
53	1983		Sulphur Baths (temp)/CSU000	15.8	5.4	0.45	0.22	0.68	0.01	0.05	10.08	2.46	0.00	3.00	0.01	0.04
54	1983		Sulphur Baths (temp)/CSU090	15.8	5.4	0.42	0.17	0.66	0.01	0.04	9.30	2.38	1.57	3.00	0.01	0.03
55	Coalinga-04	1983	Anticline Ridge Free-Field/ATC270	6.3	5.2	0.36	0.34	0.39	0.28	0.15	2.57	0.32	0.00	3.00	0.26	0.00
56		1983	Anticline Ridge Pad/ATP270	6.3	5.2	0.31	0.28	0.34	0.25	0.13	2.58	0.32	0.00	3.00	0.24	0.00
57		1983	Burnett Construction/BNT270	13.2	5.2	0.36	0.31	0.40	0.12	0.07	6.48	0.46	1.57	1.50	0.18	0.01
58		1983	Burnett Construction/BNT360	13.2	5.2	0.31	0.37	0.26	0.15	0.07	6.59	0.30	2.36	2.00	0.11	0.00
59		1983	Coalinga-14th & Elm (Old CHP)/CHP000	11.9	5.2	0.38	0.48	0.27	0.17	0.08	2.79	0.26	0.00	1.00	0.07	0.00
60		1983	Skunk Hollow/SKH270	8.9	5.2	0.31	0.40	0.23	0.18	0.05	3.54	0.24	1.57	1.50	0.07	0.00
61	1983	Skunk Hollow/SKH360	8.9	5.2	0.30	0.35	0.24	0.13	0.05	4.71	0.24	2.36	2.50	0.05	0.00	
62	Coalinga-05	1983	Oil Fields Fire Station - FF/OLF270	8.6	5.8	0.34	0.21	0.46	0.09	0.13	3.62	0.98	0.79	3.00	0.12	0.02
63		1983	Oil Fields Fire Station - Pad/OLP270	8.6	5.8	0.31	0.19	0.43	0.09	0.13	3.60	0.98	0.79	3.00	0.12	0.02
64		1983	Pleasant Valley P.P. - FF/PVP270	16.2	5.8	0.32	0.37	0.27	0.19	0.15	6.14	0.44	0.00	1.00	0.23	0.01
65		1983	Pleasant Valley P.P. - FF/PVP360	16.2	5.8	0.47	0.54	0.41	0.28	0.21	6.14	0.42	0.00	1.00	0.31	0.01
66		1983	Pleasant Valley P.P. - yard/PVY045	16.2	5.8	0.37	0.55	0.19	0.53	0.29	6.40	0.38	0.79	1.00	0.42	0.02
67		1983	Skunk Hollow/SKH270	10.0	5.8	0.36	0.37	0.34	0.31	0.17	3.69	0.36	2.36	1.50	0.29	0.01
68		1983	Transmitter Hill/TSM270	6.0	5.8	0.52	0.48	0.56	0.44	0.55	3.02	0.82	0.79	1.50	1.19	0.07
69		1983	Transmitter Hill/TSM360	6.0	5.8	0.36	0.43	0.28	0.62	0.42	3.33	0.46	0.79	1.00	0.74	0.03
70	Coalinga-06	1983	Coalinga-14th & Elm (Old CHP)/CHP000	9.3	4.9	0.41	0.42	0.39	0.11	0.06	2.24	0.36	2.36	1.00	0.07	0.00
71	Coalinga-07	1983	Coalinga-14th & Elm (Old CHP)/CHP000	9.6	5.2	0.46	0.62	0.30	0.41	0.14	2.91	0.24	1.57	3.00	0.15	0.00
72		1983	Coalinga-14th & Elm (Old CHP)/CHP090	9.6	5.2	0.61	0.73	0.50	0.68	0.36	2.90	0.34	0.79	2.00	0.70	0.02
73		1983	Sulphur Baths (temp)/CSU000	12.0	5.2	0.36	0.32	0.40	0.08	0.08	2.26	0.70	2.36	1.00	0.19	0.01
74		1983	Sulphur Baths (temp)/CSU090	12.0	5.2	0.52	0.63	0.42	0.20	0.10	2.39	0.32	0.79	1.50	0.14	0.01
75	Friuli (aftershock)	1976	ST24/x	2.0	4.5	0.40	0.34	0.46	0.05	0.03	1.95	0.38	0.79	3.00	0.09	0.00
76		1976	ST26/x	16.0	4.5	0.33	0.28	0.37	0.01	0.01	0.48	0.46	2.36	1.00	0.01	0.00
77		1976	ST26/y	16.0	4.5	0.41	0.41	0.40	0.02	0.01	0.94	0.26	0.79	2.50	0.01	0.00
78		1976	ST20/x	20.0	4.5	0.41	0.11	0.71	0.00	0.02	8.20	3.26	0.79	2.00	0.00	0.01

No.	EQ name	Year	Station name	D [km]	M _W	PI	e _a	e _v	a _p [g]	v _p [m/s]	t ₀ [s]	T _p [s]	φ [rad]	γ	S _{a,p} [g] T ₀ =0.5s	S _{a,p} [g] T ₀ =2.5s	
79	Friuli (aftershock)	1976	ST24/y	6.0	4.5	0.37	0.38	0.36	0.05	0.03	1.91	0.40	3.14	3.00	0.11	0.00	
80		1976	ST20/x	14.0	4.5	0.37	0.55	0.19	0.03	0.01	0.28	0.26	3.14	2.00	0.02	0.00	
81		1976	ST20/y	14.0	4.5	0.34	0.41	0.26	0.03	0.02	0.44	0.42	0.79	1.50	0.04	0.00	
82		1976	ST24/x	1.0	4.7	0.30	0.26	0.35	0.05	0.03	2.91	0.32	0.79	3.00	0.05	0.00	
83		1976	ST29/x	7.0	4.7	0.32	0.27	0.36	0.01	0.01	3.54	0.48	0.00	3.00	0.04	0.00	
84		1976	ST30/x	7.0	4.7	0.32	0.23	0.41	0.01	0.01	3.59	0.50	0.79	3.00	0.04	0.00	
85		1976	ST24/y	18.0	4.8	0.34	0.35	0.33	0.02	0.01	0.79	0.34	0.79	3.00	0.03	0.00	
86		1976	ST24/x	15.0	4.8	0.44	0.53	0.35	0.02	0.01	0.26	0.24	0.00	2.00	0.01	0.00	
87		1976	ST24/x	4.0	4.9	0.47	0.44	0.50	0.18	0.12	2.43	0.44	0.79	3.00	0.46	0.01	
88		1976	ST24/y	4.0	4.9	0.48	0.43	0.53	0.29	0.20	1.58	0.46	2.36	1.00	0.33	0.01	
89		1976	ST26/x	18.0	4.9	0.50	0.58	0.42	0.04	0.01	0.34	0.16	0.00	3.00	0.00	0.00	
90		1976	ST26/y	18.0	4.9	0.46	0.52	0.40	0.06	0.01	0.28	0.18	1.57	1.00	0.01	0.00	
91		1976	ST24/y	15.0	4.9	0.30	0.38	0.21	0.05	0.02	1.81	0.32	0.79	3.00	0.04	0.00	
92		1976	ST33/y	11.0	4.9	0.40	0.52	0.28	0.03	0.01	3.01	0.28	0.00	2.50	0.02	0.00	
93		1976	ST33/x	9.0	5.5	0.72	0.73	0.72	0.20	0.27	2.55	0.76	0.00	1.50	0.63	0.03	
94		1976	ST33/y	9.0	5.5	0.41	0.38	0.44	0.07	0.10	3.00	0.76	0.00	2.00	0.23	0.01	
95		1976	ST24/x	15.0	5.5	0.41	0.29	0.54	0.09	0.10	3.50	0.62	0.00	1.50	0.26	0.01	
96		1976	ST24/y	15.0	5.5	0.55	0.54	0.55	0.23	0.14	4.20	0.40	2.36	3.00	0.45	0.01	
97		1976	ST24/y	14.0	6.0	0.43	0.40	0.45	0.25	0.21	3.92	0.56	1.57	3.00	0.93	0.02	
98		1977	ST24/x	7.0	5.4	0.46	0.44	0.47	0.18	0.11	3.02	0.40	2.36	3.00	0.35	0.01	
99		1977	ST28/x	7.0	5.4	0.34	0.46	0.22	0.07	0.04	2.31	0.32	2.36	3.00	0.07	0.00	
100		1977	ST28/y	7.0	5.4	0.33	0.45	0.22	0.08	0.04	2.31	0.30	0.79	3.00	0.06	0.00	
101		1977	ST1043/y	11.0	5.4	0.33	0.29	0.36	0.08	0.07	2.15	0.54	2.36	2.50	0.26	0.00	
102		1977	ST309/x	9.0	5.4	0.46	0.54	0.37	0.18	0.06	1.85	0.34	1.57	1.00	0.10	0.00	
103		Ionian	1973	ST8/x	15.0	5.8	0.67	0.71	0.64	0.52	0.66	3.61	0.88	2.36	1.00	1.44	0.08
104			1973	ST8/y	15.0	5.8	0.40	0.34	0.47	0.19	0.33	3.30	1.00	3.14	1.00	0.54	0.05
105			1988	ST8/x	13.0	4.8	0.63	0.62	0.63	0.11	0.09	1.80	0.46	0.00	1.00	0.14	0.01
106			1988	ST8/y	13.0	4.8	0.76	0.77	0.75	0.20	0.13	2.01	0.42	1.57	3.00	0.45	0.01
107			1988	ST126/x	12.0	4.8	0.90	0.90	0.90	0.26	0.17	2.87	0.42	0.79	2.00	0.45	0.01
108	1988		ST126/y	12.0	4.8	0.58	0.57	0.59	0.08	0.05	2.78	0.42	0.79	2.50	0.16	0.00	
109	Izmit (aftershock)	1999	ST3133/x	7.0	4.9	0.45	0.29	0.61	0.04	0.03	13.41	0.48	1.57	3.00	0.12	0.00	
110		1999	ST3139/y	9.0	4.9	0.31	0.36	0.27	0.08	0.02	13.31	0.14	1.57	3.00	0.01	0.00	
111		1999	ST3136/x	14.0	4.9	0.52	0.41	0.62	0.16	0.07	13.92	0.28	0.79	3.00	0.10	0.00	
112		1999	ST3136/y	14.0	4.9	0.64	0.59	0.68	0.32	0.14	13.52	0.28	2.36	3.00	0.20	0.00	
113	Kefallinia island	1992	ST1303/y	14.0	5.6	0.49	0.45	0.53	0.17	0.12	2.76	0.40	0.00	1.50	0.22	0.01	
114	Montenegro	1979	ST64/y	15.0	5.4	0.48	0.50	0.45	0.06	0.04	1.83	0.50	0.79	1.00	0.08	0.00	
115		1979	ST67/x	16.0	6.9	0.44	0.38	0.50	0.28	0.44	9.72	1.10	1.57	3.00	0.37	0.08	
116	Montenegro (aftershock)	1979	ST73/y	8.0	6.2	0.38	0.39	0.37	0.25	0.29	2.65	0.68	0.00	2.00	0.81	0.03	
117	Montenegro, Yugo.	1979	Bar-Skupstina Opstine/BSO000	10.9	7.1	0.44	0.38	0.50	0.28	0.45	9.64	1.10	1.57	3.00	0.37	0.08	
118		1979	Ulcinj - Hotel Olimpic/ULO090	14.7	7.1	0.42	0.28	0.56	0.17	0.42	3.23	1.60	0.79	2.50	0.20	0.16	
119	Niigata, Japan	2004	NIG019/NS	4.4	6.6	0.33	0.30	0.36	0.73	0.99	22.28	0.82	0.00	3.00	1.58	0.10	
120	Northridge-01	1994	LA - Sepulveda VA Hospital/SPV270	8.5	6.7	0.47	0.40	0.53	0.61	0.89	3.59	0.96	2.36	1.50	1.40	0.14	
121		1994	LA - Wonderland Ave/WON185	19.0	6.7	0.36	0.22	0.51	0.10	0.16	8.20	1.10	0.79	1.00	0.24	0.02	
122		1994	LA 00/LA0270	14.4	6.7	0.33	0.30	0.35	0.34	0.33	14.01	0.54	0.00	1.00	0.61	0.03	
123		1994	LA Dam/LDM064	11.8	6.7	0.33	0.32	0.35	0.32	0.62	2.81	1.36	2.36	1.00	0.58	0.12	
124		1994	Pacoima Kagel Canyon/PKC360	19.3	6.7	0.32	0.37	0.28	0.38	0.37	3.70	0.72	1.57	2.00	1.13	0.04	
125		1994	Rinaldi Receiving Sta/RRS228	10.9	6.7	0.56	0.48	0.63	0.84	1.14	2.67	1.34	1.57	1.00	1.60	0.25	

No.	EQ name	Year	Station name	D [km]	M _w	PI	e _a	e _v	a _p [g]	v _p [m/s]	t ₀ [s]	T _p [s]	φ [rad]	γ	S _{a,p} [g] T ₀ =0.5s	S _{a,p} [g] T ₀ =2.5s
126	Northridge-01	1994	Simi Valley - Katherine Rd/KAT000	12.2	6.7	0.32	0.27	0.38	0.38	0.41	5.22	0.74	1.57	3.00	0.98	0.04
127		1994	Sun Valley - Roscoe Blvd/RO3090	12.4	6.7	0.31	0.33	0.29	0.32	0.39	3.93	1.20	1.57	1.00	0.67	0.07
128		1994	Sylmar - Converter Sta/SCS142	13.1	6.7	0.48	0.43	0.54	0.55	1.22	6.60	1.46	2.36	1.50	0.70	0.33
129		1994	Sylmar - Converter Sta East/SCE281	13.6	6.7	0.34	0.28	0.41	0.31	0.53	6.50	1.38	1.57	1.50	0.40	0.16
130		1994	Beverly Hills - 14145 Mulhol/MUL009	13.4	6.7	0.37	0.28	0.47	0.28	0.50	8.80	1.14	2.36	3.00	0.37	0.09
131		1994	Jensen Filter Plant Administrative Building/JEN022	13.0	6.7	0.32	0.30	0.35	0.29	0.93	3.43	1.82	0.00	1.00	0.42	0.24
132		1994	Jensen Filter Plant Administrative Building/JEN292	13.0	6.7	0.45	0.39	0.50	0.41	0.84	5.64	1.32	2.36	3.00	0.49	0.22
133		1994	LA - Chalon Rd/CHL160	14.9	6.7	0.33	0.31	0.35	0.16	0.21	8.42	0.82	0.79	3.00	0.35	0.02
134		1994	LA - N Faring Rd/FAR000	17.0	6.7	0.30	0.25	0.36	0.16	0.18	5.24	0.72	2.36	3.00	0.46	0.02
135		Northridge-02	1994	Pacoima Kagel Canyon/PKC360	11.1	6.1	0.41	0.48	0.34	0.07	0.03	4.06	0.26	1.57	2.50	0.03
136	Northridge-03	1994	Newhall - Fire Sta/NWH180	9.1	5.2	0.63	0.65	0.60	0.20	0.19	3.02	0.62	2.36	1.50	0.55	0.02
137	Northridge-06	1994	Beverly Hills - 12520 Mulhol/MU2035	13.3	5.3	0.36	0.33	0.40	0.15	0.06	3.07	0.26	2.36	3.00	0.07	0.00
138		1994	Beverly Hills - 12520 Mulhol/MU2125	13.3	5.3	0.34	0.28	0.39	0.12	0.06	3.07	0.30	0.79	3.00	0.09	0.00
139		1994	Burbank - Howard Rd./HOW060	16.2	5.3	0.55	0.52	0.57	0.06	0.05	2.75	0.40	0.00	1.50	0.09	0.00
140		1994	Burbank - Howard Rd./HOW330	16.2	5.3	0.62	0.47	0.77	0.04	0.03	2.64	0.48	2.36	3.00	0.11	0.00
141		1994	Burbank - N Buena Vista/BUE250	15.0	5.3	0.33	0.26	0.40	0.13	0.06	3.87	0.32	0.79	1.50	0.09	0.00
142		1994	Burbank - N Buena Vista/BUE340	15.0	5.3	0.48	0.40	0.57	0.14	0.09	3.99	0.40	0.00	2.50	0.26	0.00
143		1994	Hollywood - Wiloughby Ave/WIL180	18.9	5.3	0.62	0.49	0.75	0.06	0.05	3.96	0.56	1.57	3.00	0.23	0.00
144		1994	Jensen Filter Plant Administrative Building/JEN022	9.2	5.3	0.60	0.52	0.68	0.18	0.16	2.94	0.86	1.57	1.00	0.48	0.02
145		1994	Jensen Filter Plant Administrative Building/JEN292	9.2	5.3	0.45	0.46	0.43	0.21	0.15	3.11	0.48	1.57	3.00	0.66	0.01
146		1994	Jensen Filter Plant Generator Building/JGB022	9.3	5.3	0.45	0.39	0.52	0.17	0.16	2.83	0.64	0.79	1.00	0.34	0.02
147		1994	Jensen Filter Plant Generator Building/JGB292	9.3	5.3	0.55	0.53	0.58	0.29	0.20	3.00	0.44	0.79	2.00	0.54	0.01
148		1994	LA - N Faring Rd/FAR000	16.3	5.3	0.57	0.40	0.74	0.06	0.05	3.65	0.64	1.57	3.00	0.20	0.00
149		1994	LA - N Faring Rd/FAR090	16.3	5.3	0.37	0.46	0.29	0.10	0.04	3.63	0.26	0.79	2.00	0.05	0.00
150		1994	LA - Wonderland Ave/WON095	15.7	5.3	0.56	0.44	0.68	0.04	0.02	3.02	0.28	0.79	3.00	0.02	0.00
151		1994	LA - Wonderland Ave/WON185	15.7	5.3	0.53	0.51	0.56	0.04	0.02	3.12	0.34	2.36	2.50	0.05	0.00
152		1994	Northridge - 17645 Saticoy St/STC090	4.6	5.3	0.40	0.41	0.39	0.17	0.09	2.96	0.34	2.36	2.00	0.16	0.00
153		1994	Pacoima Kagel Canyon/PKC090	11.7	5.3	0.34	0.36	0.32	0.14	0.11	2.84	0.42	0.00	1.50	0.22	0.01
154		1994	Panorama City - Roscoe/RO2180	3.2	5.3	0.48	0.44	0.52	0.12	0.06	3.41	0.30	0.79	2.50	0.09	0.00
155		1994	Rinaldi Receiving Sta/RRS228	5.5	5.3	0.44	0.38	0.50	0.48	0.33	2.09	0.44	2.36	2.50	1.09	0.02
156		1994	Simi Valley - Katherine Rd/KAT090	17.9	5.3	0.48	0.46	0.50	0.09	0.05	1.33	0.34	2.36	3.00	0.10	0.00
157		1994	Sun Valley - Roscoe Blvd/RO3090	5.1	5.3	0.45	0.33	0.58	0.08	0.09	3.43	0.66	0.00	1.00	0.18	0.01
158		1994	Sun Valley - Sunland/SUL230	10.0	5.3	0.59	0.61	0.56	0.35	0.14	3.29	0.30	1.57	2.00	0.25	0.01
159		1994	Sun Valley - Sunland/SUL320	10.0	5.3	0.75	0.73	0.76	0.24	0.10	3.38	0.30	1.57	2.50	0.19	0.00
160		1994	Sylmar - Converter Sta/SCS052	9.0	5.3	0.53	0.39	0.68	0.13	0.16	3.27	0.74	0.00	2.50	0.38	0.02
161		1994	Sylmar - Converter Sta/SCS142	9.0	5.3	0.65	0.54	0.76	0.23	0.17	2.98	0.56	1.57	2.00	0.66	0.02
162		1994	Sylmar - Converter Sta East/SCE281	9.0	5.3	0.30	0.33	0.27	0.10	0.04	3.42	0.26	0.00	3.00	0.05	0.00
163		1994	Sylmar - Sayre St/SAY045	9.0	5.3	0.50	0.39	0.61	0.16	0.11	2.70	0.50	1.57	2.00	0.39	0.01
164		1994	Sylmar - Sayre St/SAY315	9.0	5.3	0.53	0.45	0.60	0.22	0.15	2.66	0.40	0.00	1.00	0.22	0.01
165		1994	Sylmar - Olive View Med FF/SYL090	10.9	5.3	0.35	0.30	0.40	0.13	0.09	4.48	0.48	1.57	2.00	0.30	0.01
166		1994	LA - UCLA Grounds/UCL360	18.5	5.3	0.30	0.16	0.44	0.06	0.04	3.84	0.54	1.57	3.00	0.20	0.00
167		1994	LA - Sepulveda VA Hospital/SPV000	2.0	5.3	0.39	0.38	0.39	0.26	0.17	3.32	0.36	0.00	1.50	0.27	0.01
168		1994	LA - Chalon Rd/CHL070	16.2	5.3	0.30	0.36	0.23	0.07	0.03	3.93	0.30	2.36	3.00	0.06	0.00
169		1994	LA - Chalon Rd/CHL160	16.2	5.3	0.64	0.50	0.78	0.04	0.04	3.61	0.66	2.36	3.00	0.14	0.00
170		1994	Canoga Park - Topanga Can/CNP106	12.2	5.3	0.32	0.28	0.35	0.09	0.04	5.93	0.32	1.57	3.00	0.08	0.00
171		1994	Canoga Park - Topanga Can/CNP196	12.2	5.3	0.47	0.43	0.51	0.22	0.16	4.00	0.50	0.79	1.00	0.31	0.01
172		1994	Studio City - Ventura & Coldwater Cyn Av/CO2182	11.1	5.3	0.47	0.30	0.64	0.15	0.12	3.63	0.54	1.57	3.00	0.55	0.01

No.	EQ name	Year	Station name	D [km]	M _w	PI	e _a	e _v	a _p [g]	v _p [m/s]	t ₀ [s]	T _p [s]	φ [rad]	γ	S _{a,p} [g] T ₀ =0.5s	S _{a,p} [g] T ₀ =2.5s
173	Northridge-06	1994	N Hollywood - Coldwater Can/CWC180	7.1	5.3	0.30	0.37	0.24	0.12	0.04	2.51	0.24	1.57	3.00	0.04	0.00
174		1994	Chatsworth - Devonshire/DEV000	16.6	5.3	0.34	0.36	0.31	0.17	0.08	2.47	0.28	0.00	3.00	0.11	0.00
175		1994	Chatsworth - Devonshire/DEV090	16.6	5.3	0.50	0.39	0.61	0.20	0.12	3.87	0.40	2.36	1.50	0.24	0.01
176	Point Mugu	1973	Port Hueneme/PHN180	18.1	5.7	0.36	0.35	0.37	0.10	0.14	1.09	0.98	0.79	1.00	0.26	0.02
177	Racha (aftershock)	1991	ST199/x	11.0	5.6	0.45	0.42	0.49	0.35	0.23	7.17	0.64	1.57	1.00	0.71	0.02
178		1991	ST199/y	11.0	5.6	0.43	0.47	0.40	0.54	0.25	6.50	0.30	2.36	3.00	0.43	0.01
179	San Fernando	1971	Pacoima Dam (upper left abut)/PUL164	11.9	6.6	0.31	0.16	0.46	0.42	0.99	3.18	1.56	0.79	1.50	0.52	0.29
180	San Francisco	1957	Golden Gate Park/GGP010	11.1	5.3	0.37	0.35	0.40	0.06	0.02	1.49	0.30	1.57	3.00	0.04	0.00
181	SE of Tirana	1988	ST2368/y	7.0	5.9	0.44	0.61	0.27	0.35	0.11	4.67	0.30	1.57	1.00	0.14	0.00
182	Sierra Madre	1991	Altadena - Eaton Canyon/ALT000	12.6	5.6	0.55	0.56	0.53	0.39	0.27	2.80	0.42	0.00	3.00	0.90	0.01
183		1991	Altadena - Eaton Canyon/ALT090	12.6	5.6	0.31	0.28	0.33	0.10	0.08	3.08	0.50	0.79	3.00	0.35	0.00
184		1991	Cogswell Dam - Right Abutment/COG155	18.8	5.6	0.32	0.40	0.24	0.25	0.11	1.88	0.30	1.57	3.00	0.19	0.00
185		1991	Pasadena - USGS/NSMP Office/SMP270	18.0	5.6	0.40	0.51	0.30	0.19	0.12	3.07	0.38	0.00	3.00	0.33	0.00
186		1991	Pasadena - USGS/NSMP Office/SMP360	18.0	5.6	0.38	0.49	0.26	0.21	0.13	3.26	0.40	0.79	3.00	0.39	0.01
187		1991	San Marino - SW Academy/SMA090	20.0	5.6	0.36	0.31	0.41	0.10	0.11	3.40	0.60	3.14	1.00	0.21	0.01
188	Spitak (aftershock)	1989	ST180/y	16.0	5.2	0.30	0.23	0.37	0.01	0.01	1.25	0.48	2.36	3.00	0.04	0.00

Table S3: Near-source, pulse-like ground motions from strike-slip faults and the parameters of the extracted pulses.

Legend	
D	Epicentral distance
M_W	moment magnitude
PI	pulse indicator
e_a	matching index for the extracted acceleration pulse
e_v	matching index for the obtained velocity pulse
a_p	amplitude of the acceleration pulse
v_p	corresponding velocity amplitude of the elementary wavelet
t_0	time instance when the acceleration pulse starts
T_p	period of the pulse
φ	phase of the elementary wavelet
γ	parameter that controls the oscillatory character of the elementary wavelet
S_a	pseudoacceleration of an elastic SDoF oscillator

The pulses that result in larger pseudoaccelerations of the two elastic SDoF oscillators with $T_0=0.5$ and 2.5s than those of recorded ground motions are shown in **bold font**

Earthquake Records from
Strike-Slip Faults

No.	EQ name	Year	Station name	D [km]	M_W	PI	e_a	e_v	a_p [g]	v_p [m/s]	t_0 [s]	T_p [s]	φ [rad]	γ	$S_{a,p}$ [g] $T_0=0.5s$	$S_{a,p}$ [g] $T_0=2.5s$
1	Ancona	1972	ST3/x	8.0	4.7	0.43	0.27	0.59	0.20	0.15	1.50	0.50	2.36	3.00	0.65	0.01
2	Anza (Horse Canyon)-01	1980	Anza - Pinyon Flat/PFT135	12.7	5.2	0.51	0.32	0.69	0.07	0.04	2.21	0.52	1.57	1.00	0.10	0.00
3	Bam, Iran	2003	Bam/L	12.6	6.6	0.46	0.17	0.75	0.41	1.19	2.75	1.98	2.36	1.00	0.48	0.34
4	Chalfant Valley-01	1986	Zack Brothers Ranch/ZAK360	10.5	5.8	0.32	0.39	0.25	0.20	0.18	4.13	0.54	0.00	3.00	0.76	0.01
5	Chalfant Valley-02	1986	Zack Brothers Ranch/ZAK360	14.3	6.2	0.38	0.34	0.42	0.29	0.39	3.98	0.86	0.79	3.00	0.55	0.05
6	Coyote Lake	1979	Coyote Lake Dam - SW Abutment/CYC250	8.0	5.7	0.53	0.59	0.46	0.24	0.18	1.82	0.48	2.36	2.50	0.64	0.01
7		1979	Gilroy Array #2/G02140	10.9	5.7	0.30	0.31	0.30	0.23	0.24	3.62	0.72	0.79	1.00	0.52	0.03
8		1979	Gilroy Array #3/G03050	9.6	5.7	0.32	0.23	0.40	0.10	0.17	3.72	1.12	2.36	3.00	0.13	0.03
9		1979	Gilroy Array #3/G03140	9.6	5.7	0.43	0.31	0.56	0.16	0.27	3.11	1.20	0.79	1.00	0.35	0.04
10		1979	Gilroy Array #4/G04360	7.7	5.7	0.31	0.34	0.28	0.22	0.27	2.65	0.70	0.00	1.00	0.56	0.03
11		1979	Gilroy Array #6/G06230	4.4	5.7	0.61	0.57	0.65	0.30	0.47	2.44	0.88	0.00	1.00	0.88	0.06
12		1979	Gilroy Array #6/G06320	4.4	5.7	0.44	0.54	0.34	0.32	0.18	2.27	0.36	2.36	3.00	0.43	0.01
13	Darfield, New Zealand	2010	DSL/N63E	13.4	7.0	0.44	0.10	0.79	0.05	0.55	19.96	6.94	0.79	3.00	0.05	0.06
14		2010	GDLC/S35W	4.4	7.0	0.39	0.28	0.50	0.37	0.88	17.29	1.92	1.57	1.50	0.43	0.40
15	Erzincan, Turkey	1992	ST205/x	13.0	6.6	0.56	0.55	0.58	0.30	1.03	2.89	1.94	0.00	1.00	0.42	0.27
16		1992	Erzincan/ERZ-NS	9.0	6.7	0.57	0.55	0.59	0.29	1.02	2.80	1.96	0.00	1.00	0.39	0.28
17	Faial	1998	ST87/x	11.0	6.1	0.40	0.33	0.47	0.30	0.30	4.10	0.64	2.36	2.50	1.08	0.02
18		1998	ST87/y	11.0	6.1	0.42	0.32	0.51	0.32	0.40	4.04	0.84	0.79	1.00	0.83	0.05
19	Firuzabad	1994	ST3290/x	20.0	5.9	0.37	0.36	0.39	0.03	0.01	2.78	0.18	0.79	3.00	0.01	0.00
20	Gilroy	2002	Gilroy - Gavilan Coll./GIL337	2.8	4.9	0.35	0.36	0.35	0.18	0.04	7.13	0.14	0.00	2.50	0.02	0.00
21	Hollister-03	1974	Hollister City Hall/HCH181	9.8	5.1	0.31	0.35	0.27	0.10	0.05	2.52	0.38	1.57	2.50	0.14	0.00
22		1974	Hollister City Hall/HCH271	9.8	5.1	0.37	0.41	0.33	0.15	0.08	1.52	0.40	1.57	3.00	0.28	0.00
23	Ierissos	1983	ST1311/x	8.0	5.1	0.46	0.39	0.53	0.09	0.06	2.30	0.40	2.36	3.00	0.18	0.00
24		1983	ST1328/y	15.0	5.1	0.45	0.56	0.33	0.13	0.05	2.54	0.24	1.57	3.00	0.09	0.00
25	Imperial Valley-06	1979	EI Centro - Meloland Geot. Array/EMO000	19.4	6.5	0.41	0.44	0.37	0.24	0.57	4.97	1.34	0.00	1.00	0.52	0.11
26		1979	EI Centro - Meloland Geot. Array/EMO270	19.4	6.5	0.63	0.52	0.74	0.18	0.89	4.94	2.82	0.00	1.50	0.19	0.46
27	Imperial Valley-07	1979	Bonds Corner/BCR140	12.7	5.0	0.34	0.23	0.45	0.03	0.03	4.38	0.60	2.36	2.50	0.11	0.00
28		1979	Bonds Corner/BCR230	11.9	5.0	0.65	0.50	0.80	0.06	0.09	4.57	0.96	2.36	1.50	0.13	0.01
29		1979	Calxico Fire Station/CXO225	11.9	5.0	0.67	0.64	0.69	0.10	0.07	3.37	0.70	1.57	1.00	0.23	0.01
30		1979	Calxico Fire Station/CXO315	12.0	5.0	0.32	0.30	0.35	0.06	0.05	3.54	0.60	0.79	1.00	0.10	0.00
31		1979	EI Centro Array #10/E10050	12.0	5.0	0.49	0.37	0.61	0.04	0.03	3.06	0.50	0.00	2.50	0.11	0.00

No.	EQ name	Year	Station name	D [km]	M _W	PI	e _a	e _v	a _p [g]	v _p [m/s]	t ₀ [s]	T _p [s]	φ [rad]	γ	S _{a,p} [g] T ₀ =0.5s	S _{a,p} [g] T ₀ =2.5s
32	Imperial Valley-07	1979	EI Centro Array #11/E11140	14.5	5.0	0.35	0.33	0.37	0.08	0.07	4.14	0.64	0.79	1.00	0.15	0.01
33		1979	EI Centro Array #11/E11230	14.5	5.0	0.81	0.80	0.82	0.16	0.12	3.86	0.44	0.00	2.50	0.37	0.01
34		1979	EI Centro Array #2/E02140	18.0	5.0	0.81	0.73	0.89	0.14	0.10	3.94	0.70	1.57	1.00	0.31	0.01
35		1979	EI Centro Array #2/E02230	18.0	5.0	0.35	0.36	0.34	0.07	0.04	3.83	0.38	0.79	1.00	0.05	0.00
36		1979	EI Centro Array #3/E03140	15.3	5.0	0.71	0.64	0.77	0.12	0.12	3.83	0.66	0.79	1.00	0.26	0.01
37		1979	EI Centro Array #3/E03230	15.3	5.0	0.46	0.56	0.36	0.09	0.05	3.81	0.30	0.00	1.00	0.05	0.00
38		1979	EI Centro Array #4/E04140	10.9	5.0	0.58	0.59	0.56	0.19	0.12	3.19	0.36	0.00	1.00	0.16	0.01
39		1979	EI Centro Array #4/E04230	10.9	5.0	0.53	0.49	0.57	0.11	0.07	3.41	0.42	2.36	3.00	0.24	0.00
40		1979	EI Centro Array #5/E05140	10.1	5.0	0.56	0.58	0.55	0.19	0.09	3.42	0.46	1.57	1.00	0.20	0.01
41		1979	EI Centro Array #5/E05230	10.1	5.0	0.56	0.49	0.64	0.15	0.12	3.45	0.56	0.79	1.00	0.25	0.01
42		1979	EI Centro Array #6/E06140	9.1	5.0	0.63	0.56	0.70	0.15	0.15	4.80	0.66	0.79	1.00	0.32	0.02
43		1979	EI Centro Array #6/E06230	9.1	5.0	0.69	0.63	0.74	0.28	0.25	4.43	0.62	2.36	1.00	0.56	0.02
44		1979	EI Centro Differential Array/EDA270	9.4	5.0	0.57	0.48	0.67	0.15	0.11	4.53	0.52	0.79	1.00	0.22	0.01
45		1979	EI Centro Differential Array/EDA360	9.4	5.0	0.39	0.23	0.54	0.10	0.08	4.50	0.54	2.36	1.00	0.16	0.01
46		Javakheti Highland	1990	ST193/x	20.0	5.4	0.48	0.50	0.45	0.03	0.02	7.60	0.34	1.57	3.00	0.05
47	Kobe, Japan	1995	KJM/000	18.3	6.9	0.30	0.26	0.33	0.71	1.10	8.44	1.06	0.79	1.00	1.75	0.16
48		1995	KJM/090	18.3	6.9	0.43	0.40	0.46	0.58	0.71	8.02	0.86	1.57	2.50	1.21	0.10
49		1995	Port Island (0 m)/PRI000	19.3	6.9	0.35	0.45	0.25	0.26	0.59	8.86	1.46	2.36	2.50	0.31	0.19
50		1995	Port Island (0 m)/PRI090	19.3	6.9	0.36	0.48	0.23	0.21	0.41	8.46	1.22	0.79	3.00	0.27	0.09
51		1995	Takatori/000	13.1	6.9	0.40	0.34	0.46	0.56	1.49	5.97	1.74	2.36	1.50	0.64	0.49
52		1995	Takatori/090	13.1	6.9	0.32	0.27	0.37	0.41	0.86	5.60	1.44	1.57	3.00	0.48	0.27
53	Kocaeli, Turkey	1999	Yarimca/YPT060	19.3	7.5	0.43	0.21	0.65	0.09	0.63	11.43	4.62	2.36	2.50	0.09	0.16
54		1999	Yarimca/YPT150	19.3	7.5	0.33	0.18	0.48	0.08	0.46	12.28	3.74	1.57	3.00	0.09	0.21
55	Kyllini (aftershock)	1988	ST172/x	19.0	4.5	0.32	0.48	0.17	0.04	0.02	2.53	0.38	2.36	1.50	0.03	0.00
56		1988	ST172/x	16.0	4.5	0.45	0.38	0.51	0.03	0.02	2.75	0.40	0.79	3.00	0.06	0.00
57		1988	ST172/y	19.0	4.5	0.30	0.42	0.19	0.03	0.02	2.79	0.42	3.14	1.50	0.04	0.00
58		1988	ST172/y	16.0	4.5	0.61	0.49	0.73	0.05	0.04	2.87	0.56	2.36	1.00	0.09	0.00
59		1988	ST1359/x	14.0	4.8	0.33	0.30	0.37	0.04	0.02	2.61	0.32	2.36	3.00	0.03	0.00
60		1988	ST172/y	17.0	4.8	0.38	0.44	0.32	0.03	0.02	3.62	0.40	1.57	3.00	0.06	0.00
61	Livermore-02	1980	Livermore - Morgan Terr Park/LMO355	10.3	5.4	0.31	0.46	0.16	0.29	0.10	3.04	0.22	2.36	3.00	0.08	0.00
62	Mammoth Lakes-05	1980	Convict Creek/CVK090	9.4	5.7	0.42	0.40	0.43	0.08	0.09	1.88	0.60	0.00	1.00	0.17	0.01
63	Mammoth Lakes-07	1980	Long Valley Fire Sta/XLV000	4.6	4.7	0.44	0.25	0.63	0.02	0.02	1.29	1.00	1.57	1.50	0.03	0.00
64	Mammoth Lakes-10	1983	Convict Creek/CVK090	8.9	5.3	0.47	0.43	0.50	0.12	0.14	2.31	0.72	0.00	2.50	0.37	0.01
65		1983	Convict Creek/CVK180	8.9	5.3	0.46	0.31	0.61	0.10	0.17	2.14	1.18	0.79	1.00	0.23	0.03
66	Mammoth Lakes-11	1983	Convict Creek/CVK180	9.8	5.3	0.33	0.19	0.47	0.03	0.06	2.26	1.14	1.57	3.00	0.05	0.01
67	Morgan Hill	1984	Anderson Dam (Downstream)/AND250	16.7	6.2	0.40	0.47	0.32	0.33	0.21	4.78	0.48	1.57	2.00	0.74	0.02
68		1984	Anderson Dam (Downstream)/AND340	16.7	6.2	0.35	0.41	0.28	0.28	0.28	4.80	0.60	0.00	2.00	0.90	0.02
69		1984	Halls Valley/HVR240	3.9	6.2	0.49	0.39	0.59	0.28	0.44	10.47	1.10	2.36	1.00	0.70	0.07
70	Mt. Hengill Area	1998	ST2495/y	18.0	5.4	0.33	0.34	0.32	0.03	0.04	13.12	0.68	0.00	2.00	0.10	0.00
71		1998	ST2496/x	18.0	5.4	0.38	0.17	0.58	0.01	0.01	6.29	1.58	2.36	1.00	0.01	0.00
72		1998	ST2497/y	15.0	5.4	0.49	0.35	0.64	0.01	0.02	15.02	1.56	1.57	3.00	0.01	0.01
73		1998	ST2556/x	15.0	5.4	0.44	0.18	0.69	0.01	0.02	8.04	1.90	2.36	2.50	0.01	0.01
74		1998	ST2556/y	15.0	5.4	0.39	0.22	0.56	0.01	0.02	4.25	1.60	0.79	3.00	0.01	0.01
75	Northwest China-01	1997	Jiashi/JIA270	13.2	5.9	0.44	0.40	0.48	0.24	0.17	5.74	0.44	2.36	3.00	0.62	0.01
76	Parkfield	1966	CO2/065		6.2	0.33	0.50	0.15	0.41	0.36	4.00	0.60	1.57	3.00	1.48	0.03
77	Parkfield-02, CA	2004	Parkfield - Cholame 1E/C01090	11.4	6.0	0.56	0.42	0.71	0.20	0.32	2.98	1.32	1.57	1.50	0.27	0.09
78		2004	Parkfield - Cholame 1E/C01360	11.4	6.0	0.54	0.49	0.58	0.27	0.34	2.77	0.84	0.79	1.50	0.70	0.04

No.	EQ name	Year	Station name	D [km]	M _w	PI	e _a	e _v	a _p [g]	v _p [m/s]	t ₀ [s]	T _p [s]	φ [rad]	γ	S _{a,p} [g] T ₀ =0.5s	S _{a,p} [g] T ₀ =2.5s
79	Parkfield-02, CA	2004	Parkfield - Cholame 2WA/C02090	11.5	6.0	0.67	0.60	0.74	0.44	0.64	3.10	0.94	2.36	1.50	1.06	0.09
80		2004	Parkfield - Cholame 2WA/C02360	11.5	6.0	0.45	0.47	0.42	0.37	0.40	2.92	0.70	2.36	1.50	1.08	0.04
81		2004	Parkfield - Cholame 3E/TM3090	11.9	6.0	0.60	0.53	0.67	0.30	0.23	2.72	0.46	0.00	3.00	0.88	0.01
82		2004	Parkfield - Cholame 3E/TM3360	11.9	6.0	0.42	0.35	0.49	0.50	0.23	2.63	0.46	1.57	1.00	0.53	0.02
83		2004	Parkfield - Cholame 3W/C03090	12.2	6.0	0.40	0.27	0.53	0.18	0.19	2.89	0.86	1.57	1.50	0.46	0.03
84		2004	Parkfield - Cholame 3W/C03360	12.2	6.0	0.52	0.41	0.64	0.30	0.31	2.89	1.04	1.57	1.00	0.74	0.04
85		2004	Parkfield - Cholame 4W/C04090	12.3	6.0	0.35	0.38	0.32	0.47	0.24	2.85	0.50	1.57	1.00	0.58	0.02
86		2004	Parkfield - Cholame 4W/C04360	12.3	6.0	0.48	0.49	0.47	0.39	0.24	2.79	0.60	1.57	1.00	0.70	0.02
87		2004	Parkfield - Cholame 5W/C05360	13.8	6.0	0.30	0.22	0.37	0.11	0.13	8.31	0.70	0.00	2.50	0.34	0.01
88		2004	Parkfield - EADES/090	10.0	6.0	0.41	0.21	0.62	0.16	0.23	5.18	1.42	1.57	1.00	0.28	0.06
89		2004	Parkfield - EADES/360	10.0	6.0	0.41	0.23	0.59	0.15	0.23	3.89	0.94	0.79	2.50	0.27	0.03
90		2004	Parkfield - Fault Zone 1/COW090	8.4	6.0	0.34	0.40	0.27	0.52	0.59	3.83	0.78	0.79	1.00	1.27	0.07
91		2004	Parkfield - Fault Zone 1/COW360	8.4	6.0	0.62	0.53	0.71	0.41	0.80	3.43	1.08	0.00	1.50	0.87	0.13
92		2004	Parkfield - Fault Zone 12/PRK090	11.0	6.0	0.53	0.50	0.55	0.26	0.37	3.35	0.98	1.57	3.00	0.37	0.06
93		2004	Parkfield - Fault Zone 12/PRK360	11.0	6.0	0.60	0.51	0.69	0.26	0.49	2.72	1.24	0.79	1.50	0.39	0.09
94		2004	Parkfield - Fault Zone 9/Z09090	10.0	6.0	0.65	0.54	0.75	0.14	0.23	2.67	1.28	1.57	1.50	0.21	0.06
95		2004	Parkfield - Fault Zone 9/Z09360	10.0	6.0	0.37	0.31	0.44	0.09	0.12	2.73	1.08	1.57	1.50	0.17	0.02
96		2004	Parkfield - HOG CANYON/HOG360	0.8	6.0	0.30	0.26	0.35	0.20	0.19	10.41	0.76	1.57	1.50	0.56	0.02
97		2004	Parkfield - Stone Corral 1E/SC1090	7.2	6.0	0.36	0.30	0.43	0.44	0.37	2.23	0.58	2.36	1.00	0.78	0.03
98		2004	Parkfield - Stone Corral 1E/SC1360	7.2	6.0	0.36	0.39	0.33	0.60	0.25	2.21	0.42	1.57	1.00	0.53	0.02
99	Patras	1993	ST10/y	10.0	5.6	0.31	0.32	0.31	0.15	0.11	5.41	0.46	0.79	1.50	0.27	0.01
100	Patras (aftershock)	1993	ST10/y	11.0	4.6	0.33	0.50	0.16	0.03	0.01	3.00	0.16	2.36	2.00	0.01	0.00
101		1993	ST1330/y	11.0	4.6	0.43	0.67	0.20	0.07	0.02	2.97	0.14	0.79	3.00	0.02	0.00
102	Pyrgos	1996	ST214/x	2.0	4.7	0.34	0.36	0.32	0.09	0.03	3.18	0.32	1.57	1.00	0.04	0.00
103		1996	ST214/y	2.0	4.7	0.40	0.50	0.30	0.12	0.03	3.12	0.20	1.57	3.00	0.03	0.00
104	Pyrgos (aftershock)	1993	ST214/x	20.0	4.5	0.40	0.50	0.30	0.02	0.02	3.21	0.46	2.36	1.00	0.03	0.00
105		1993	ST214/y	20.0	4.5	0.40	0.51	0.30	0.04	0.02	3.13	0.42	1.57	1.00	0.03	0.00
106		1993	ST159/y	14.0	4.7	0.40	0.45	0.36	0.05	0.02	3.32	0.26	2.36	2.00	0.03	0.00
107	Pyrgos (foreshock)	1993	ST214/x	1.0	4.9	0.40	0.35	0.44	0.07	0.05	4.11	0.38	0.00	1.50	0.09	0.00
108		1993	ST214/x	7.0	4.9	0.39	0.42	0.36	0.09	0.03	2.86	0.24	0.79	3.00	0.06	0.00
109		1993	ST214/y	7.0	4.9	0.34	0.27	0.40	0.06	0.03	2.74	0.34	1.57	3.00	0.10	0.00
110	San Salvador	1986	Geotech Investig Center/GIC090	7.9	5.8	0.32	0.43	0.20	0.66	0.43	1.58	0.64	1.57	1.00	1.32	0.04
111		1986	Geotech Investig Center/GIC180	7.9	5.8	0.44	0.51	0.37	0.33	0.42	1.74	0.76	0.00	3.00	0.89	0.04
112		1986	National Geographical Inst/NGI180	9.5	5.8	0.50	0.46	0.55	0.29	0.61	2.09	1.46	0.79	1.00	0.51	0.13
113		1986	National Geographical Inst/NGI270	9.5	5.8	0.66	0.60	0.72	0.42	0.52	2.22	0.84	1.57	3.00	0.84	0.07
114	South Iceland	2000	ST2486/x	5.0	6.5	0.44	0.23	0.64	0.19	0.54	13.90	1.96	0.79	1.00	0.22	0.15
115	South Iceland (aftershock)	2000	ST2483/y	6.0	6.4	0.67	0.46	0.88	0.26	0.77	12.13	1.96	0.79	1.50	0.28	0.32
116		2000	ST2488/y	11.0	6.4	0.67	0.48	0.86	0.38	0.92	13.31	1.68	0.79	1.00	0.50	0.23
117		2000	ST2556/y	20.0	6.4	0.36	0.30	0.43	0.03	0.11	16.43	2.46	2.36	3.00	0.03	0.10
118		2000	ST2558/x	5.0	6.4	0.36	0.40	0.33	0.60	0.39	12.55	0.44	0.79	1.00	0.55	0.02
119	Superstition Hills-02	1987	Kornbloom Road (temp)/KRN360	19.3	6.5	0.53	0.34	0.72	0.11	0.32	5.63	1.92	0.79	1.00	0.13	0.09
120		1987	Parachute Test Site/PTS225	16.0	6.5	0.49	0.37	0.61	0.30	0.91	12.29	1.96	0.79	2.50	0.33	0.49
121	Tottori, Japan	2000	TTR008/EW	16.5	6.6	0.53	0.48	0.58	0.26	0.53	10.31	1.30	0.79	3.00	0.32	0.13
122	Westmorland	1981	Westmorland Fire Sta/WSM090	7.0	5.9	0.37	0.22	0.52	0.20	0.36	5.62	1.30	1.57	2.50	0.25	0.10
123		1981	Westmorland Fire Sta/WSM180	7.0	5.9	0.40	0.38	0.43	0.31	0.38	5.88	0.74	0.00	3.00	0.88	0.03
124	Yountville	2000	Napa Fire Station #3/2016A090	9.9	5.0	0.63	0.52	0.73	0.41	0.49	13.09	0.82	2.36	1.00	1.12	0.05
125		2000	Napa Fire Station #3/2016B360	9.9	5.0	0.33	0.38	0.27	0.44	0.31	13.25	0.40	3.14	1.00	0.44	0.02